DocDays VT 2024

Book of Abstracts

JULY 1st & 2nd, 2024

Graz University of Technology

DocDay VT & Minisymposium 2024 Program

Monday 1st July 2024

Time	Activity	Location
9:00 - 9:30	***Registration***	**Lobby**
9:30 - 9:40	***Welcome/Opening Session*** **Moderation: Ulrich Hirn**	**HS i9**
	Research Proposals – Session A: Advanced Process Engineering and Simulation **Chair: Heidrun Gruber-Wölfler**	**HS i9**
9:40 – 10:00	***Continuous Flow Syntheses of Covalent Organic Frameworks*** *Michael König*	
10:00 – 10:20	***Efficient Hybrid Modeling for Sustainable Processes: Integrating Mechanistic Insights and Machine Learning*** *Michael Mitterlindner*	
10:20 – 10:40	***Development of CFD surrogate reactor models for optimization, control and scale-up of gassed and stirred tanks*** *Lukas Gsenger*	
10:40 – 11:00	***Uncertainty Quantification of DEM Simulations*** *Lukas Maier*	
	Research Proposals – Session B: Biomaterials and Chemical Processes **Chair: Wolfgang Bauer**	**HS i8**
9:40 – 10:00	***Efficient Decentralised Electrochemical Methanol Production (Gas to Methanol)*** *Hafiz Farooq Imtiaz*	
10:00 – 10:20	***All-cellulose composites as precursors for activated carbon***	

Time	Activity	Location
	Alexa Scheer	
10:20 – 10:40	***Lignin Isolation and its Implementation in Epoxy Resin Production*** *Sebastian Sandner*	
11:00 – 11:30	***Coffee Break***	**Lobby**
	Research Proposals – Session C: Efficient Hydrogen Production and Energy Storage **Chair: Viktor Hacker**	**HS i8**
11:30 – 11:50	***Optimization of the SO2 depolarized electrolyser for more economic, less energy intensive alternative hydrogen production*** *Lukas Fernando Roessler Escudero*	
11:50 – 12:10	***System Modeling of a Fixed-Bed Chemical Looping Hydrogen Process for Energy Storage*** *Claudia Pröll*	
12:10 – 12:30	***Component-based degradation routes on PEM water electrolysis*** *Özge Kiziltan*	
	Research Proposals – Session D: Innovations in Fuel Cell Technology **Chair: Merit Bodner**	**HS i9**
11:30 – 11:50	***Mitigating Over-Humidification Risks for Enhanced Performance and Durability of Fuel Cell-Powered Electric Vehicles*** *Maximilian Käfer*	
11:50 – 12:10	***Investigation of Advanced Membrane Electrode Assemblies in High Temperature Polymer Electrolyte Fuel Cells for Heavy Duty Vehicle Applications*** *Florian Tritscher*	

Time	Activity	Location
12:10 – 12:30	***Development of Membrane Electrode Assembly (MEA) with Modified Nanofiber Structure*** *Muhammad Yusro*	
12:30 – 13:30	**Lunch Break**	
13:30 – 14:00	***Q&A Administrative Aspects of the Doctoral Studies*** **Moderation: Heidrun Gruber-Woelfler**	**HS i9**
	Session 1: Fiber- and Cellulose Engineering **Chair: Marlene Kienberger**	**HS i9**
14:00 – 14:20	***Fractionation of wood due to industrial chipping – Effects and potential for Kraft pulping of European spruce*** *Roman Poschner*	
14:20 – 14:40	***Comparison of Film Press and Spray Application of Polysaccharide Based Coatings on Paper and Board*** *Anna Mayrhofer*	
14:40 – 15:00	***Probing interfacial interactions – Ionic liquids and cellulose*** *Lukas Pachernegg*	
	Session 2: Innovative Processes for Waste Stream Recycling / Upcycling **Chair: Hans Schnitzer**	**HS i8**
14:00 – 14:20	***Characterization and isolation of molecules from tomato plant residues using sustainable green solvents*** *Adrian Drescher*	
14:20 – 14:40	***Electrochemical Investigation of Symmetric Aminoquinones*** *Janine Maier*	

Time	Activity	Location
14:40 – 15:00	***Polymer recycling solutions for textile waste containing elastane*** *Emanuel Boschmeier*	
15:00 – 15:30	***Coffee Break***	**Lobby**
	Session 3: Advances in CO_2 Sequestration and Utilization **Chair: Thomas Gamse**	**HS i8**
15:30 – 15:50	***CO2-Sequestration of MSWI residues via direct, aqueous carbonation*** *Sarah Reiter*	
15:50 – 16:10	***CO2 utilization by catalytic hydrogenation*** *Kamonrat Suksumrit*	
	Session 4: Innovations in Process Design and Optimization **Chair: Thomas Wallek**	**HS i9**
15:30 – 15:50	***Novel Concepts for Processing and Automation of Pharmaceutical End-to-End Manufacturing*** *Lisa Kuchler*	
15:50 – 16:10	***Continuous hydrolysis in oscillatory flow rheology as process intensification strategy for biorefineries*** *Judith Buchmaier*	
16:10 – 17:10	***Poster Session (+ best poster/presentation voting)***	**HS i9 / Lobby**
17:10 - 20:00	**Social Event - Barbeque**	

Poster Session

1) ***Solvent extraction of aromatic aldehydes from biorefinery side-streams***

   Alexander Kaufmann

2) ***Advances in Photometric Fluoride Measurements in Effluent Fuel Cell Water***

   Mathias Heidinger

3) ***Aging gracefully? Shelf-life investigations of catalyst ink for polymer electrolyte fuel cells***

   Mario Kircher

4) ***A versatile method for quantifying porous carbonaceous material in different wastewater matrices***

   Christian Margreiter

5) ***Production of activated carbon: Thermal activation of gasification char***

   David Gurtner

6) ***Characterization of pyrometallurgical systems by electrochemical methods***

   Simon Moll

7) ***Experimental study on stirrer scale-up in the 2-20 liter range***

   Thomas Senfter

8) ***Life cycle-oriented cost assessment of an integrated energy system***

   Doris Rixrath

9) ***Mixed-Matrix Membranes on the way to Multi-Layer Membranes***

   Jana Marx

10) ***The reverse water gas shift reaction: Investigation of the reaction with nickel and perovskite based catalysts***

    Marion Andritz

11) ***Utilizing Pressure-Driven Membrane Processes for Concentrating Sugar Solution***

    Eva Walcher

12) ***Composition of textiles waste in Vienna***

    Pablo Kählig

Tuesday 2nd July 2024

Time	Activity	Location
9:00 – 10:00	*Keynote Presentation: 20 Years of Carbonate Based Ionic Liquids Synthesis (CBILS®): A Startup Journey from a Greek Beach towards World Leadership in Manufacture of Ionic Liquids* **Keynote speaker: Roland Kalb** **Moderation: Ulrich Hirn**	**HS i9**
10:00 – 10:30	***Coffee Break***	
	Session 5: Modeling and Simulation in Engineering / Particle Forum **Chair: Stefan Radl**	**HS i9**
10:30 – 10:50	***Robot-LDA line measurements on a 30° inclined flat plate in an open wind channel with and without plasma actuation effect*** *Manuel Berger*	
10:50 – 11:10	***Application of a novel hybrid multi-scale model in a fluidized bed with an immersed tube*** *Behrad Esgandari*	
11:10 – 11:30	***A Random Forest modeling approach for packed column hydraulics*** *Marcus Schlager*	
11:30 – 11:50	***Discrete Modeling of Interlocking and Cohesive Bulk Solids using Tetrapods*** *Stefan Radl*	
	Session 6: Advancements in Gas Processing and Biomass Gasification Technologies **Chair: Gernot Krammer**	**HS i8**
10:30 – 10:50	***Design of gas disperser for power to gas processes in bubble columns***	

	Florian Klapal	
10:50 – 11:10	***Load-flexible biogas methanation in a cooled tube reactor*** *Katrin Salbrechter*	
11:10 – 11:30	***Comparative Assessment of Solid Phase Adsorption Methodologies for Tar Quantification in Biomass Gasification*** *Michael Kresta*	
11:50 – 12:20	***Coffee Break***	**Lobby**
12:20 – 12:50	*Awards and Closing Session* **Moderation: Ulrich Hirn**	**HS i9**
	Best Presentation Award Best Poster Award	

Oral Presentations

Session 1 – Fiber and Cellulose Engineering

July 1, 2024 14:00 – 15:00

Lecture Hall: i9

Chairperson: Prof. Marlene Kienberger

14:20

Fractionation of wood due to industrial chipping – Effects and potential for Kraft pulping of European spruce

Presenting Author: Roman Poschner

Roman Poschner, Lukas Hopf, Caterina Czibula, Adelheid Bakhshi, Thomas Harter, Rene Eckhart, Ulrich Hirn
Institute of Bioproducts and Paper Technology, Graz University of Technology, Inffeldgasse 23, 8010 Graz, Austria
corresponding author: ulrich.hirn@tugraz.at

The research conducted on kraft cooking of different chip sizes is often not representative for the industrial process since the chip size fractions were made of high-quality wood without impurities. We evaluated the effects and the potential of cooking non ideal spruce chip fractions after industrial chipping and screening. The chips were classified according to SCAN 40:01, and the respective fractions were cooked under the identical conditions to mimic the effect of a joint cooking in the industrial digester. For the undersized chips we found higher bark content, a lower screened yield, a higher Kappa number, lower fiber length and lower tensile strength. For the oversized chips, the fiber length and tensile index were also considerably lower. A lower wood quality due to high knot content in the larger fractions was found to be the reason for that. Based on the data obtained from the experiments and literature, different process options for increased yield and reduced chemical consumption are discussed, e.g., separate cooking of different chip fractions. Improved chip screening seems to be the process improvement with lowest costs and highest impact.

14:20

Comparison of Film Press and Spray Application of Polysaccharide Based Coatings on Paper and Board

Presenting Author: Anna Mayrhofer

Comparison of Film Press and Spray Application of Polysaccharide Based Coatings on Paper and Board

Mayrhofer, A.[1,*], Mandlez, D.[1], Harter, T. [1] and Bauer, W. [1]
[1] Institute of Bioproducts and Paper Technology, Graz University of Technology, Graz, Austria
* anna.mayrhofer@tugraz.at

Food packaging materials must fulfill several objectives, such as providing gas, grease, and oil barriers to protect goods from spoiling. Paper and board are well-established materials for packaging foods due to their high recycling rate and biodegradability but require additional modifications to achieve the desired barrier properties. In conventional packaging these barrier properties are often achieved by applying layers of non-renewable materials such as plastics or metal films, and the resulting composites pose significant environment challenges.

Naturally occurring biopolymers like alginate and chitosan have shown potential as effective barriers in food packaging applications. However, their application on paper and board poses several challenges to state-of-the-art paper coating equipment caused, especially due to their high viscosity already at low solids content.

This research demonstrates the potential of spray application for polysaccharides to overcome some of the difficulties associated with conventional paper and board coating methods in applying these materials.

Coating results and barrier properties generally are highly dependent on the suitable combination of solution and base paper substrate properties. We compare coating materials with varying viscosities and surface tensions applied to paper substrates with different surface energies using both film press and spray coating techniques. Whilst the aqueous biopolymer solutions used are difficult to spray onto hydrophobized surfaces, the spray application on un-hydrophobized papers shows advantages compared to the film press application. Contrary to film press coating, the coat weight of a spray coater is not limited by the coating aggregate and, with sufficient wetting, can provide an even coating layer in a single application step on the surface, which is crucial for barrier performance.

Although several challenges remain, our results indicate that spray applications of polysaccharide-based barrier materials are a promising method to apply high viscous biopolymer solutions to paper and board for food packaging applications.

14:40

Probing interfacial interactions – Ionic liquids and cellulose

Presenting Author: Lukas Pachernegg

Pachernegg, L.[1,2,*], Schaubeder, J.[1], Czibula, C.[1], Coclite, A.M.[3], Hirn, U.[1], Spirk, S. [1,2]
[1] Institute of Bioproducts and Paper Technology, University of Technology, Graz, Austria
[2] Ecolyte GmbH, Inffeldgasse 21b, Graz, Austria
[3] Institute of Solid State Physics, University of Technology, Graz, Austria
*presenter/corresponding author: lpachernegg@tugraz.at

Cellulose is earths most abundant biopolymer and has broad applications ranging from simple products to high performance applications in medicine. Many of these applications need solutions for shaping and modification of the cellulose which often require complex solvent combinations or the derivatization of cellulose. (Sayyed et al., 2019) Ionic liquids offer an easier pathway for direct dissolution of cellulose.

However, the interactions of cellulose and ionic liquids are still not fully understood. Here we demonstrate how the use of contact angle measurements and its modelling on cellulose model films can help to better understand the interactions. Further AFM is used to revile the hierarchical structure of cellulose and how the interactions take place and influence the mechanical properties. Our studies showed how the ionic liquids are spreading on the surface of the cellulose and which parameters influence the efficient spreading of the cellulose. Further we were able to demonstrate via AFM how the ionic liquid is dissolving the cellulose, starting from its primary wall (Figure 1).

This work contributes to our understanding of the interactions between cellulose and ionic liquids. Investigating the underlying mechanisms is crucial for future developments of ionic liquids as well as enhancing processes.

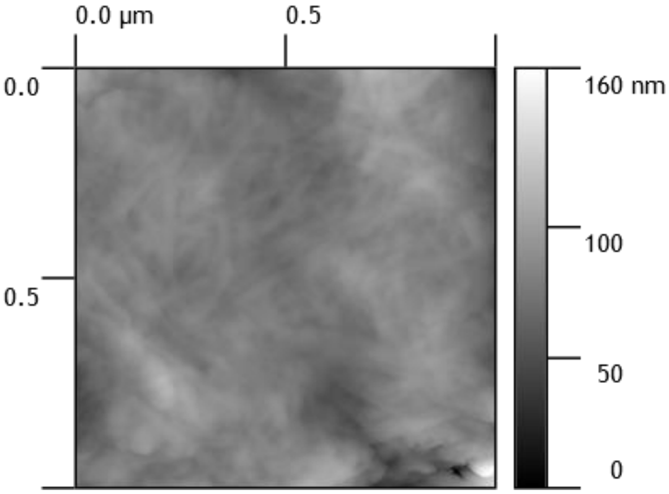

Figure 1: Single flax fiber after treatment for 1h with ionic liquid in ambient temperature.

References:

[1] Sayyed, A. J., Deshmukh, N. A., & Pinjari, D. V. (2019). A critical review of manufacturing processes used in regenerated cellulosic fibres: viscose, cellulose acetate, cuprammonium,

LiCl/DMAc, ionic liquids, and NMMO based lyocell. Cellulose, 26(5), 2913-2940. https://doi.org/10.1007/s10570-019-02318-y

Session 2 – Innovative Processes for Waste Stream Recycling / Upcycling

July 1, 2024 14:00 – 15:00

Lecture Hall i8

Chairperson: Prof. Hans Schnitzer

14:00

Characterization and isolation of molecules from tomato plant residues using sustainable green solvents

Presenting Author: Adrian Drescher

Drescher, A.[1, *], Schwingshackl, L., Donauer, M., Kaufmann, M.[1] and Kienberger, M.[1]
[1] Institute of Chemical Engineering and Environmental Technology, Graz University of Technology, Inffeldgasse 25C, 8010 Graz; adrian.drescher@tugraz.at
*presenter/corresponding author: adrian.drescher@tugraz.at

Graphical abstract

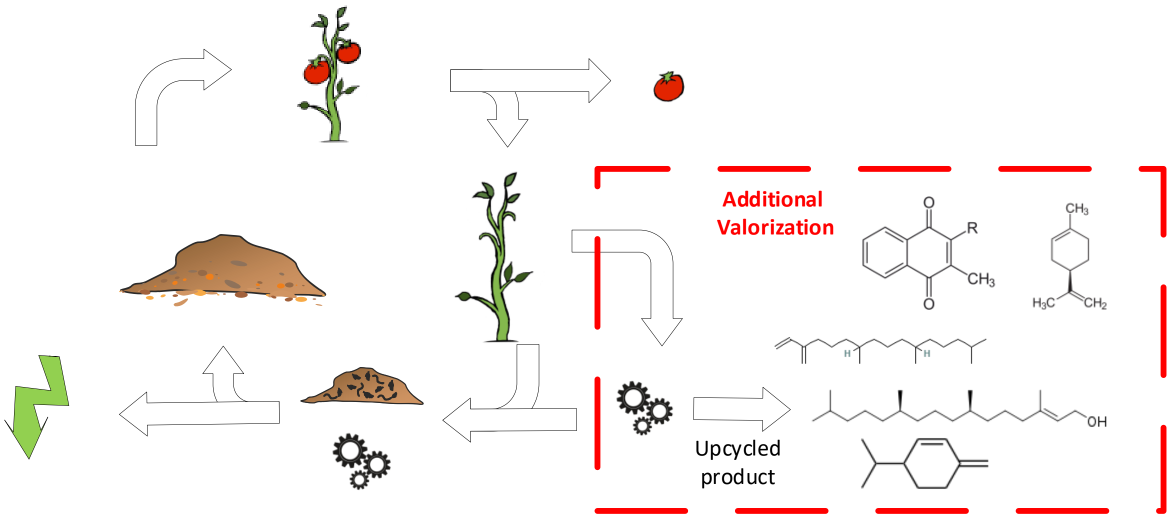

Figure 2: Advanced tomato plant residue valorization cycle

Tomatoes (Solanum lycopersicum) are the second most produced and consumed vegetable globally, with production of nearly 189 million tons over 5.16 million hectares, mostly in greenhouses. This production generates significant waste, approximately 252.84 million tons of residues like stems, leaves, and green cull tomatoes. These residues, often disposed improperly, can block riverbeds, emit greenhouse gases, and pose toxicity risks to livestock while spreading pathogens to other plants.

Fruits and vegetables, including tomatoes, are known for containing bioactive compounds such as terpenes, terpenoids, polyphenols, and fatty acids, which have pharmaceutical and health benefits. Research has extensively covered these compounds in fruits, but less in agricultural by-products. For tomatoes, most studies focus on seeds and peels rather than the vegetative parts. Extracting valuable compounds from residues typically involves non-green or toxic solvents.

This study aims to fill this gap by characterizing and extracting molecules from tomato plant residues using environmentally friendly solvents (e.g., ethanol, methyl-tetrahydrofuran (m-THF), ethyl acetate, and supercritical CO2). Various extraction methods, including solid-liquid, vacuum-assisted Soxhlet, and supercritical CO2 extraction, were employed.

Samples of air-dried tomato plant material (4-6 g, 2-5 mm size) were prepared for extraction using supercritical CO2, hexane, ethanol, m-THF, ethyl acetate, and a hexane-ethanol mixture. For solid-liquid extraction, a 1:10 weight-to-volume ratio was used, with samples shaken in a water bath at 50°C for 24 hours. Vacuum-assisted Soxhlet extraction was performed at 50°C under 260-510 mbara pressure. Supercritical CO2 extraction included blending the plant material with 3 wt% sunflower oil and extracting at 40-80°C and 10-30 MPa pressures.

Extracts were analysed with gas chromatography mass spectrometry (GC-MS) and a modified Folin-Ciocalteu method for total phenolic content (TPC), measuring absorbance at 765 nm.

GC-MS analysis identified 285 compounds in five classes: 42 hydrocarbons, 6 phenolic compounds, 63 fatty acids and esters, 34 terpenes and terpenoids, and 140 uncategorized compounds. In m-THF and hexane extracts, fatty acids and esters dominated, while ethanol, ethyl acetate, and ethanol-hexane mixtures were rich in terpenes and terpenoids. Supercritical CO2 extracts were primarily hydrocarbons. Key compounds included tetracontane, squalene, cannabidiol, neophytadiene, and vitamin E, noted for their antimicrobial and antioxidant properties.

The solvents 2-MTHF and ethyl acetate outperformed ethanol and hexane, yielding a maximum of 99 ± 8.83 compounds. They achieved a maximum total concentration of 5,894.82 ± 586.48 mg NEQ/kgdw and 3,363.02 ± 71.14 mg NEQ/kgdw, respectively, and a TPC of 2,143.25 ± 155.17 mg GAE/kgdw and 1,605.92 ± 66.46 mg GAE/kgdw. Neophytadiene was the most abundant terpene, with concentrations of 781.2 ± 112.66 mg NEQ/kgdw in ethyl acetate and 718.25 ± 54.89 mg NEQ/kgdw in 2-MTHF extracts. Supercritical CO2, which can be compared with hexane according to its polarity, extracted a 73% lower total concentration, but a 107% higher TPC compared to hexane.

The study highlights the diverse bioactive compounds in tomato plant residues and the potential for green solvents like m-THF and ethyl acetate to enhance their extraction. However, economic extraction processes face challenges due to low compound quantities, influenced by plant growth conditions. Further research should explore system boundaries and additional processing methods such as fermentation to optimize extraction and find new valorization paths.

14:20

Electrochemical Investigation of Symmetric Aminoquinones

Presenting Author: Janine Maier

Maier, J.[1,2,*], Yagmur R. [1,2], Wickenhauser D. [1,2], Kelterer A-M.[3], Torvisco A.[4] and Spirk S.[1,2]
[1] Institute of Bioproducts and Paper Technology, Graz University of Technology, Inffeldgasse 23, 8010 Graz, Austria
[2] Ecolyte GmbH, Inffeldgasse 21B, 8010 Graz, Austria
[3] Institute of Physical and Theoretical Chemistry, Stremayrgasse 9/I, 8010 Graz, Austria
[4] Institute of Inorganic Chemistry Graz, University of Technology, Stremayrgasse 9/IV, 8010 Graz, Austria
*presenter/corresponding author: janine.maier@tugraz.at

Quinones have a wide range of valuable properties and potential applications in medicinal chemistry, materials science, optoelectronic devices, and batteries. Molecular redesign using different functional groups, like amines, can optimize their properties and prevent unwanted side reactions.

However, particularly the synthesis of aminoquinones can be challenging at times, and there is a need for simple and efficient routes to access these compounds without metal catalysts or halogenated starting materials.
Here, we demonstrate the synthesis and electrochemical characterization of a series of aminoquinones derived from renewable sources, namely vanillin or 2-methoxyhydroquinone.[1]
We employ a series of primary and secondary amines, varying in their electronic situation as well as steric demand. Depending on the type of starting material, either the desired aminoquinone or the related Schiff-base adduct was obtained. The aminoquinones were further explored for their stability at different pH values. At extreme pH values, the deeply colored aminoquinones decompose, accompanied by decolorization of the solutions within a few minutes (pH 14) or hours (pH 1). At intermediate pH values (3-8) the aminoquinones are stable upon storage in solution, where they feature a quasi-reversible redox chemistry and fast, diffusion limited kinetics.[2]

Figure 1. Redox reaction of symmetric aminoquinones

Acknowledgement: We acknowledge funding from the Austrian Research Promotion Agency (FFG, 883933). This research has also received funding from the European Innovation Council (EIC) under grant agreement No. 101115293 (VanillaFlow).

References:

[1] a) W. Schlemmer, P. Nothdurft, A. Petzold, G. Riess, P. Frühwirt, M. Schmallegger, G. Gescheidt-Demner, R. Fischer, S. A. Freunberger, W. Kern, and S. Spirk, *Angew. Chem. Int. Ed.*, **59**, 22943 (2020). b) M. Barbero, V. A. Papillo, A. A. Grolla, R. Negri, F. Travaglia, M. Bordiga, F. Condorelli, M. Arlorio, and G. B. Giovenzana, *Eur. J. Org. Chem.*, **2020**, 136-139 (2020).

[2] S. Bayen, N. Barooah, R. J. Sarma, T. K. Sen, A. Karmakar, and J. B. Baruah, *Dyes Pigm.*, **75**, 770 (2007).

Session 3 – Advances in CO_2 Sequestration and Utilization

July 1, 2024 15:30 – 16:10

Lecture Hall i8

Chairperson: Prof. Thomas Gamse

15:30

CO_2-Sequestration of MSWI residues via direct, aqueous carbonation

Reiter, S.[1,*], Schinnerl, F.[1], Lehner, M.[1]
[1] Chair of Process Engineering and Environmental Protection, Montanuniversität Leoben, Austria
*Presenter/corresponding author: sarah.reiter@unileoben.ac.at

Introduction and Objectives

The continuously increasing concentration of CO_2 in the atmosphere necessitates technological solutions to mitigate its emissions [1]. Among these, methods of CO_2 capture, utilization, and storage (CCUS) are gaining prominence, especially for addressing 'hard-to-abate' emissions that persist despite reduction efforts [2]. One promising approach for carbon dioxide storage is mineral carbonation, which is based on an in nature occurring process known as silicate weathering. This process involves the reaction between rocks rich in calcium oxide (CaO) and/or magnesium oxide (MgO) bearing minerals and atmospheric CO_2, resulting in the formation of stable carbonates. Carbonates are recognized as the most thermodynamically stable derivative of carbon dioxide, enabling long-term CO_2 storage and thus making the carbonation reaction particularly relevant for CO_2 mitigation [1]. Additionally, various industrial solid residues, including municipal solid waste incineration (MSWI) ash, iron and steel slag, cement dust, and residues from the construction and refractory industries, offer potential sources of calcium or magnesium oxides, thereby making carbonation a pertinent option for industries seeking to mitigate CO_2 emissions [3].
The most promising route for CO_2-storage in alkaline residues is direct aqueous carbonation [4], where water acts as a solvent for the gaseous CO_2 and the Ca- or Mg-oxides in the solid material [3, 5]. Increased temperatures and pressure facilitate mineral and gas dissolution and therefore aid carbonate precipitation [6].

This study aims to explore the CO_2-sequestration potential of residues from an Austrian MSWI plant with grate firing via direct, aqueous carbonation. Mild process parameters simulate carbonation with flue gas at ambient conditions, while more intense conditions target process optimization. Given that these residues are currently landfilled, carbonation endeavors to mitigate CO_2 emissions of the MSWI plant by repurposing its own waste streams.

Materials and Methods

In total, four residues were investigated for the study, including two designated as bottom ash, which represent the ash passing through the grate during firing. The remaining samples are termed bottom slag, representing the sintered residue accumulating at the end of the grate. All samples are either investigated in their native state (original) or ground via a ball mill, with subsequent separation of the 90-125 µm fraction for experimental utilization.

The bottom slag samples include both fresh and aged variants. The fresh sample was collected at the MSWI plant, one month prior to the commencement of the carbonation experiments, and was stored in a gas-tight container under argon atmosphere to prevent any oxidation of the material. The 6-month-old aged sample, collected in May 2023, was stored at ambient conditions in an exsiccator to prevent any water absorption. Both samples originally exhibited a particle size ranging up to a few centimeters.

The bottom ash samples are categorized into fine and coarse fractions, with the fine fraction already comprising particles ranging between 90-125 µm, requiring no further preparation.

Compositional analysis utilizing X-ray fluorescence (XRF) analysis is provided in Table 1. Thermogravimetric analysis (TGA) was used to quantify carbonate content, where CaO_{free} represents the difference between the total CaO content and the portion bound within $CaCO_3$, thereby excluding it from participation in the carbonation reaction.

Table 1: Composition and theoretical CO_2-uptake of the four MSWI samples

Species	Unit	Bottom slag fresh	Bottom slag aged	Bottom ash fine	Bottom ash coarse
CaO_{total}	wt.-%	26.16	22.38	25.33	10.58
CaO_{free}		18.02	9.60	24.94	7.21
MgO		0.02	1.72	0	0
Fe_2O_3		15.76	18.24	7.69	4.17
$CaCO_3$		14.60	22.86	0.68	6.05
SiO_2		17.26	15.42	6.91	33.59
S		0.70	0.82	5.97	0.20
U_{th}	$kg\ t^{-1}$	228.29	194.6	238.15	79.57

To evaluate the carbonation efficiency of the investigated samples, the theoretical CO_2-uptake (U_{th}) was calculated using the method described by O’Connor et al. [7]. This calculation, presented in equation (1), defines the maximum CO_2-uptake achievable if all Ca, Fe and Mg ions in the material are converted into carbonates. The resulting values for each sample are displayed at the bottom of Table 1.

$$\boldsymbol{U_{th}} = \frac{(\sum \boldsymbol{Ca^{2+}} + \boldsymbol{Fe^{2+}} + \boldsymbol{Mg^{2+}})\boldsymbol{MM_{CO2}}}{\mathbf{10}} \tag{1}$$

Experiments are conducted within a 0.6 l batch reactor (Haage Anagram) under various conditions outlined in Table 2. Prior to experimentation, all samples are dried for 2 hours at 105 °C. Nine grams of each sample are then loaded into the reactor. For experiments 1, 6, 11 & 15, requiring dampening, samples are sprayed with water, the others are suspended in 100 ml of deionized water.

Table 2: Experimental conditions for carbonation experiments of the four MSWI-samples

Samples	Exp. No.	Temp, °C	Total pres., bar	CO_2 partial pres., bar	Particle size, µm	S/l ratio, $g\ l^{-1}$
Bottom slag	1, 6	amb.	1	0.15	original	dampened

fresh (1-5) & aged (6-10)	2, 7					90
	3, 8				90-125	
	4, 9		20			
	5, 10	100				
Bottom ash Fine (11-14) & coarse (15-18)	11, 15	amb.	1	0.15	90-125	dampened
	12, 16					90
	13, 17		20			
	14, 18	100				

The reactor is then sealed, and a mixture of 85 vol.-% N_2 and 15 vol.-% CO_2 is used to purge the reactor ten times to ensure the removal of unwanted air in the reactor. This purging is followed by the injection of the same gas mixture.

For experiments conducted at 100 °C, the reactor is heated with an electrical heating jacket prior to gas injection. For experiments utilizing pure CO_2 at a total pressure of 20 bar, the gas is injected following the same procedure as for the 1 bar experiments, using 100 vol.-% CO_2 gas. Following the 2-hour experiment duration, residual gas is removed by opening the outlet valve and the reactor is unsealed. The solid- water suspension is filtered, and the filter cake is dried for 2 hours at 105 °C. Analysis via TGA allows determination of the materials CO_2-uptake by comparing results before and after carbonation experiments. Additionally, carbonation efficiency is calculated as the ratio of experimental to theoretical CO_2-uptake.

Results and discussion

Figure 3 illustrates the experimental carbon dioxide uptake in kilograms of CO_2 per ton of feed material, along with the corresponding carbonation efficiency displayed above each bar. Both bottom slag samples exhibit similar theoretical uptakes, although the aged sample shows a slightly lower uptake due to increased carbonate content resulting from aging. The fine fraction of bottom ash exhibits the highest U_{th} owing to its elevated free CaO-content.

Under mild, damp conditions, both bottom slag samples demonstrate a comparable CO_2-uptake below 5 kg t^{-1}. Adjusting the solid-to-liquid ratio and grinding slightly enhances the uptake, however it is inferred that the prevailing process conditions are too mild for sufficient results. Increasing the pressure to 20 bar results in a CO_2 uptake of 48.7 kg t^{-1} for the fresh sample and 18.2 kg t^{-1} for the aged one, which is to be expected due to the higher CO_2 solubility. A temperature elevation from 20 to 100 °C leads to final uptakes of 59.8 and 50.4 kg t^{-1} for the fresh and aged bottom slag, respectively, representing roughly a quarter of the theoretical uptake.

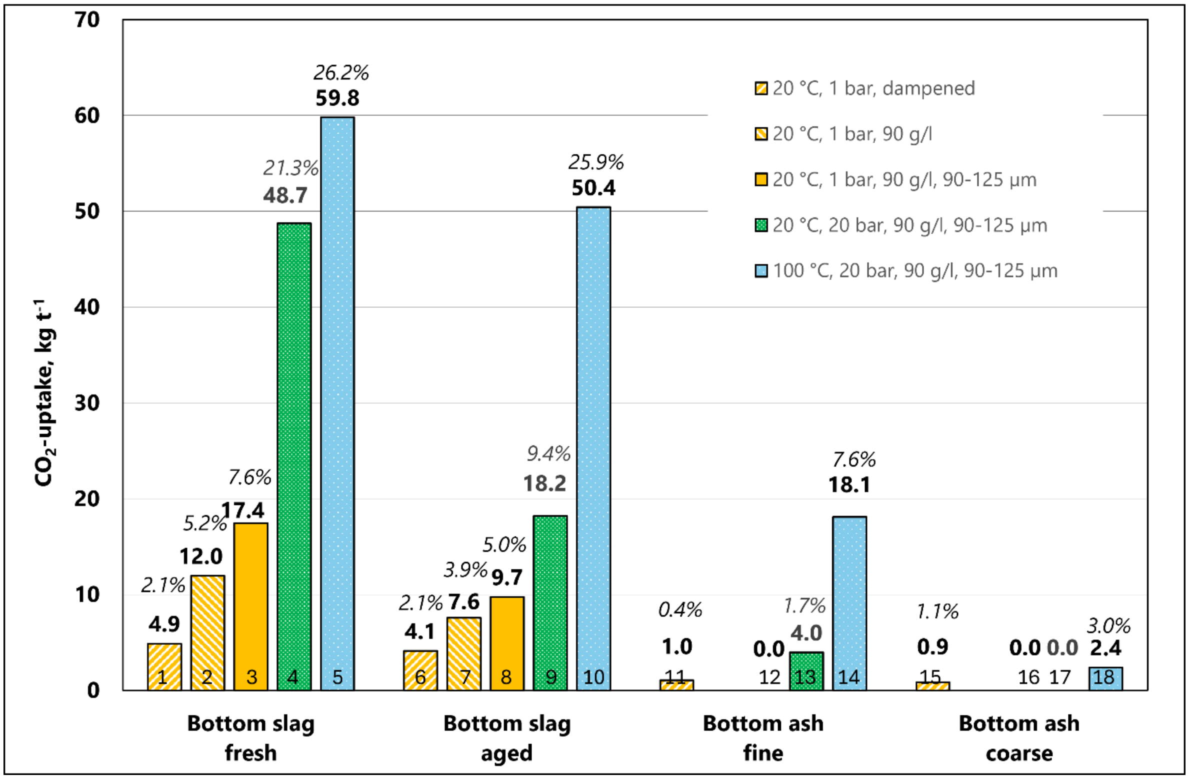

Figure 3: Experimental CO_2-uptake of the bottom slag and ash samples at different experimental conditions in kg sequestered CO_2 per ton of feed material (bold) and carbonation efficiency in % (italic)

For both the fine and coarse bottom ash, no significant CO_2-uptake can be measured for a total pressure of 1 bar. Increasing the pressure to 20 bar marginally enhances the carbonation efficiency for the fine ash. Further small improvements are achieved by raising the temperature to 100 °C, yet the maximum efficiency only reaches 7.6 and 3.0 % for the fine and coarse ash, respectively.

The diminished efficacy of the two bottom ash samples may arise from their compositions. XRF analysis reveals the fine ash's high sulfur content. Abdul et al. [3] argue, that sulfur oxides compete with the $CaCO_3$ precipitation, leading to the formation of $CaSO_3$ or $CaSO_4 \cdot 2\,H_2O$. However, this cannot be confirmed without further information about the mineral phases of the sulfur compounds. The coarse bottom ash demonstrates a notably high SiO_2 content, most likely leading to the formation of an inert silica rim around the particles, hindering further reaction with CO_2 [8, 9].

Conclusion and Outlook

The low overall experimental results of the two bottom ash samples suggest their unsuitability for carbonation. However, a definitive conclusion regarding the underlying reasons cannot be drawn without thorough examination of the present mineral phases. In contrast, the fresh and aged bottom slag samples exhibit noteworthy experimental CO_2-uptake with 59.8 and 50.4 kg CO_2 per ton feed material, respectively. Nonetheless with a total pressure of 1 bar, the process conditions do not yield satisfactory results. Besides adjustment of pressure, temperature, and particle size additional optimization strategies such as modification of solid-to-liquid ratio, reaction time or different additives hold promise for further optimizing the carbonation process and facilitating the development of an economically viable process for implementation.

References:

[1] W. Liu *et al.*, "CO2 mineral carbonation using industrial solid wastes: A review of recent developments," *Chemical Engineering Journal*, vol. 416, p. 129093, 2021, doi: 10.1016/j.cej.2021.129093.

[2] B. M. BMF, *79/21 MRV: Carbon Management – Eine Säule der österreichischen Klimapolitik: BMK*, 2023.

[3] F. Abdul, A. Iizuka, H.-J. Ho, K. Adachi, and E. Shibata, "Potential of major by-products from non-ferrous metal industries for CO2 emission reduction by mineral carbonation: a review," *Environmental science and pollution research international*, vol. 30, no. 32, pp. 78041–78074, 2023, doi: 10.1007/s11356-023-27898-y.

[4] R. Baciocchi, G. Costa, M. Di Gianfilippo, A. Polettini, R. Pomi, and A. Stramazzo, "Thin-film versus slurry-phase carbonation of steel slag: CO_2 uptake and effects on mineralogy," *Journal of hazardous materials*, vol. 283, pp. 302–313, 2015.

[5] C. Julcour, L. Cassayre, I. Benhamed, J. Diouani, and F. Bourgeois, "Insights Into Nickel Slag Carbonation in a Stirred Bead Mill," *Front. Chem. Eng.*, vol. 2, 2020, doi: 10.3389/fceng.2020.588579.

[6] A. A. Olajire, "A review of mineral carbonation technology in sequestration of CO2," *Journal of Petroleum Science and Engineering*, vol. 109, pp. 364–392, 2013, doi: 10.1016/j.petrol.2013.03.013.

[7] William Oconnor, D.C. Dahlin, G.E. Rush, S.J. Gerdemann, L.R. Penner, and D.N. Nilsen, "Aqueous Mineral Carbonation: Mineral Availability, Pretreatment, Reaction Parametrics, and Process Studies," doi: 10.13140/RG.2.2.23658.31684.

[8] H. Béarat *et al.*, "Carbon sequestration via aqueous olivine mineral carbonation: role of passivating layer formation," *Environmental science & technology*, vol. 40, no. 15, pp. 4802–4808, 2006, doi: 10.1021/es0523340.

[9] C. Julcour *et al.*, "Development of an attrition-leaching hybrid process for direct aqueous mineral carbonation," *Chemical Engineering Journal*, vol. 262, pp. 716–726, 2015, doi: 10.1016/j.cej.2014.10.031.

15:50

CO2 utilization by catalytic hydrogenation

Presenting Author: Kamonrat Suksumrit

Kamonrat Suksumrit[1,*], Susanne Lux[1]
[1] Institute of Chemical Engineering and Environmental Technology, Graz University of Technology, NAWI Graz, Inffeldgasse 25C, 8010 Graz, Austria; k.suksumrit@tugraz.at, susanne.lux@tugraz.at

*presenter/corresponding author: k.suksumrit@tugraz.at

Abstract: This research aims at identifying the influential factors that affect the efficiency and performance of carbon dioxide hydrogenation processes with heterogeneous Ni-based catalysts. These include procedures for catalyst preparation and design as well as the operation conditions of the hydrogenation reaction itself. The catalytic performance of Ni-based catalysts with two support materials i) reduced siderite ore and ii) MgO as support was evaluated and compared aiming at the exploitation of an abundant natural resource. MgO is known as an effective support material as it gives access to bifunctional catalysts because of its basicity and high CO_2 adsorption capacity.

It was demonstrated that the catalytic activity of undoped and Ni-doped reduced siderite ore for CO_2 hydrogenation at 648 K had limited methane selectivity. However, with mixed support materials ($\text{siderite}_{\text{reduced}}$/MgO) both the CO_2 conversion and the selectivity toward methane increased significantly. CO_2 conversions close to the thermodynamic equilibrium and methane selectivities of ≥95 % were achieved.

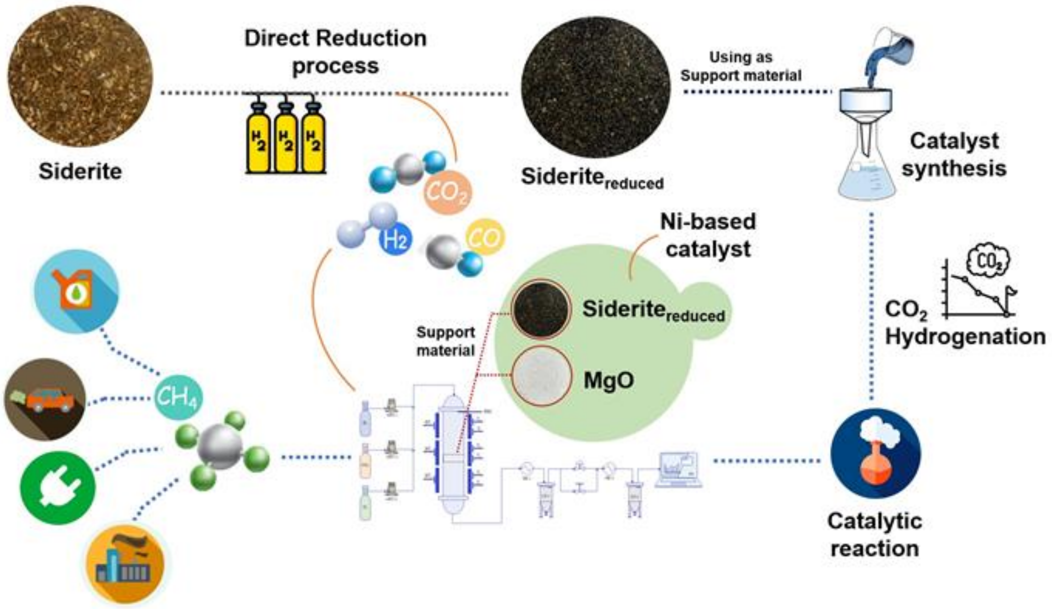

CO_2 utilization by catalytic methanation process

Session 4 – Innovations in Process Design and Optimization

July 1, 2024 15:30 – 16:10

Lecture Hall i9

Chairperson: Prof. Thomas Wallek

15:30

Novel Concepts for Processing and Automation of Pharmaceutical End-to-End Manufacturing

Presenting Author: Lisa Kuchler

Lisa Kuchler[1*], Atabak Azimi[1,2], Stefano Martinuzzi[1], Aygün Dogan[1], Simone Eder[1], Martin Spörk[1,4], Hazem Damiri[2], Martin Steinberger[2], Johannes Poms[1], Martin Kureck[3], Martin Horn[2], Johannes Khinast[1,4], Stephan Sacher[1*]
[1] Research Center Pharmaceutical Engineering GmbH, Inffeldgasse 13, 8010 Graz, Austria;
[2] Institute of Automation and Control, Graz University of Technology, Inffeldgasse 21B, 8010 Graz, Austria
[3] Evon GmbH, Wollsdorf 154, 8181 St. Ruprecht an der Raab, Austria
[4] Institute for Process and Particle Engineering, Graz University of Technology, Inffeldgasse 13/3, 8010 Graz, Austria
*Presenter: lisa.kuchler@rcpe.at
*Corresponding author: stephan.sacher@rcpe.at

In developed countries, shortages of medical products have increased dramatically in recent years. These shortages are predominantly caused by supply chain difficulties due to the geographically separated production of drug substances and drug products. The concept of end-to-end manufacturing would remedy this situation by condensing the entire manufacturing chain from API synthesis to the final dosage form at one single site[1].

In this study a continuous and automated process starting from the API synthesis to the final tablet at one single production site was developed. A novel concept has been developed for process simplification: After API synthesis in continuous flow followed by crystallization and purification, the time- and energy-intensive drying step is eliminated. The API is re-suspended instead and fed as a suspension to a hot melt extrusion (HME) step. The strand consisting of polymer and API is pelletized and tableted in a direct compaction (DC) line. The direct compaction line includes the addition of excipients to the pellets, their blending, and the subsequent tableting.

The talk will focus on the flexible control concept, which can handle different processing modes, operation modes, data acquisition strategy, and equipment scale sizes used in this end-to-end manufacturing line. Additionally, the talk also focuses on the combination of novel process routes, namely the elimination of the drying step, liquid feeding step, and the combination of HME and DC. Finally, the realization of the entire end-to-end manufacturing line in one single production room (45m^2) is also part of the presentation.

The results of the UHPLC analysis of the extrudates showed an average content of 5.20 ± 0.05 wt.% for the liquid feeding trials, which is still in an acceptable range. The results of the solid-state characterization showed that an amorphous solid dispersion (ASD) was formed, which was still stable after four weeks of storage. An average moisture content of 0.43 ± 0.05 wt.% was measured for the extrudates. This low amount of residual moisture can be neglected since no influence on the further processing of the extrudates was observed. Finally, tablets with a hardness of 110 N were produced.

The presented approach for end-to-end manufacturing allows the production of 5 kg tablets per hour in one room at 45 m² using lab to pilot scale equipment. In approximately one shift (i.e., 8 hours) the complete manufacturing chain from API raw material to the tablet can be realized.

References:

[1] Chapman, S.; Dedet, G.; Lopert, R. Shortages of medicines in OECD countries. *OECD Heal. Work. Pap.* **2022**, 1–54.

15:50

Continuous hydrolysis in oscillatory flow rheology as process intensification strategy for biorefineries

Presenting Author: Judith Buchmaier

Judith Buchmaier [1,*], Bettina Muster [1], Sofia Krampl [1], Manuel Eibinger [2], Gaurav Singh Kaira [2], Bernd Nidetzky [2].
[1] AEE - Institute for Sustainable Technologies, A-8200 Gleisdorf, Feldgasse 19
[2] Graz University of Technology, 14 Petersgasse, A- 8010 Graz, Austria
*Please address correspondence and proofs to: j.buchmaier@aee.at

In biorefining processes there are specific requirements of including reactor engineering (Brandi, Francesco 2022). New technologies ideally help in establishing highly efficient processes under sustainable conditions and meet the principles of Process Intensification (PI) and Green Chemistry (GC). GC principles include maximizing raw material conversion into products, energy-efficient design of processes as well as the prevention of waste production and disposal (Anastas, P. T., & Zimmerman, J. B 2003). Those principles align with PI aims like the replacement of traditional operations with emerging ones, creating positive impacts on space, thermodynamics, functions and time-related domains (Van Gerven und Stankiewicz 2009).

This research tackles the obstacles in sustainable biomass transformation in biorefineries, specifically focusing on enzymatic hydrolysis (Buchmaier u. a. 2020) and alkaline protein extraction. It proposes the use of continuous operation, which offers several advantages over batch processes, including reduced energy consumption and improved heat and mass transfer, leading to increased conversion yield or minimized waste. The Oscillatory Flow Bioreactor (OFB), a specially designed tubular reactor with integrated baffles is applied for bioprocesses. The OFB allows efficient mixing at high biomass solid loadings and decouples flow velocity from residence time due to the rheology at the baffle intersections, enabling continuous processing.

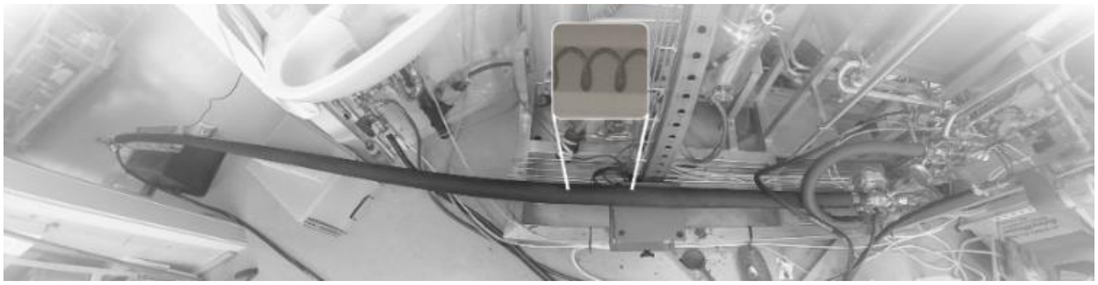

Figure 4: Oscillatory flow bioreactor as designed and used in experiments. (Photo: COFB configuration 4.5m length)

This study evaluated an adapted version of an Oscillatory Baffled Reactor (OBR), specifically the continuous oscillatory flow bioreactor (COFB) with helical baffles, for its processability and mechanical handling in extracting protein from Brewers Spent Grains (BSG). The primary objective was to facilitate direct continuous processing of an inhomogeneous bio-based substrate in oscillatory flow. Operating parameters, including solid loading, residence time, and flow velocity, were adjusted to identify the optimal operating window. This study did not aim for further downstream processing, such as acidic precipitation and isolation of the protein hydrolysate. Although Particle Image Velocimetry (PIV) and other particle imaging technologies were considered for determining flow profiles, the reactor setup and the real feedstock BSG's particle sizes (0 - 4 mm) made it unfeasible to measure and evaluate flow patterns in the non-transparent medium. Protein solubilization rates were selected as indicators to determine whether the processing goals of the COFB setup, specifically reactor length (0.89m - 4.5m) and flow velocities (110 ml/h – 1020 ml/h) at high solid loading (10% – 15% w/w), were achieved. Additionally, the BioMethane Potential (BMP) of the remaining solid biomass was explored for energy valorization, with the ultimate goal of establishing a combined resource and energy recovery process from BSG (Buchmaier u. a. 2024).

Proteins are not only crucial for humans but also for plants and animals. The bio-based industry is increasingly recognizing the potential of extracting, functionalizing, and upgrading plant proteins. Their nutritional, bioactive, and techno-functional properties make them a valuable component of bio-products. Given the rising demand for proteins, scientists and industry are looking for alternative sources. Such an alternative can be found in lignocellulosic residues from agriculture and industry. The efficient use of this available biomass through biorefinery approaches can be a way to meet the protein demand.

Brewers spent grains (BSG), a by-product of beer production, are produced in large quantities and, with their valuable components (protein content 15 – 26% DM) and physicochemical properties, have potential for biorefinery concepts. For this, there is an urgent need for efficient extraction methods and the utilization of the residual biomass.

In the present study, methodologically, in a condition screening, pre-treatment steps such as drying, sieving, and grinding were tested. As extraction methods, the combination of enzymatic and alkaline extraction was used in comparison to purely alkaline extraction. Residence Time Distribution (RTD) tests were conducted via salt addition and conductivity measurement to be able to evaluate a residence time distribution at different reactor lengths. The hydrolysates of all conducted experiments were determined via Bradford Assays for their protein concentration, and the remaining solid was collected and fed to batch fermenters to measure the biomethane potential.

The results of the study showed that the heterogeneous substrate BSG can be processed in the oscillating reactor. The pre-treatment steps tested in the condition screening showed no significant increase in protein yields in relation to the additional process technical effort and could therefore be omitted in the further extraction process. The specific requirements for the processability of high BSG contents in terms of filling, maintaining the net flow, and avoiding blockage could be achieved with the given COFB design. As an extraction method, purely alkaline extraction was chosen as it achieved 25% higher yields compared to the combined extraction method with enzymes.

The COFB was able to achieve protein extraction rates of up to 92%. On average, protein extraction rates of 65% (n=31) were achieved at high solid loadings of 10-15% BSG. This shows the COFB's great potential as a one-step extraction method for various biomass.

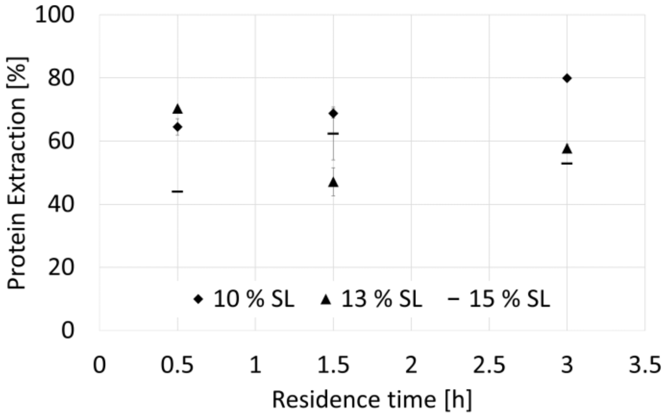

Figure 5: Protein solubilization at different residence times and solid loadings of 10 -15 % BSG (COFB; BSG in 200 mM sodium hydroxide (NaOH in dH_2O), T = 50°C, f = 1.505 Hz, x_0 = 11 mm, $l_{reactor}$= 0.89 – 3.28 m)

In this scientific work, a reactor design was developed that is capable of treating the protein-rich raw material BSG in a continuous oscillating flow. The achieved protein extraction rates are promising, and by combining the process with anaerobic digestion, biorefinery concepts for resource and energy use of an industrial waste/by-product can be developed. The process goals of this study, continuous direct biomass treatment at high solid loading (10-15 % TS BSG), were achieved. Despite limitations in characterizing the heterogeneous multiphase flow behavior, this study shows valuable results with regard to the direct and continuous treatment of biomass at high solid loading. The challenges in processing were mastered by implementing a continuous feed that can be operated at low flow rates and stable conditions without settling or blocking of particles. Protein extraction rates of an average of 65 % could be achieved over a range of different parameter settings, including residence time, flow velocity, and solid loading (Buchmaier u. a. 2024).

Certain operating conditions led to higher protein yields, but these could not be clearly linked to trends based on residence times or velocity ratios. As expected, a faster increase and higher protein concentrations were observed at higher solid loading. To the authors knowledge, this is the first report showing protein extraction from BSG in a continuous oscillating flow bioreactor.

The richness of the substrate BSG and the increasing demand for protein products make the extraction process shown here a potential biorefinery process that combines two promising approaches: “direct continuous processing of heterogeneous biomass with high solid content” and “plant-based protein extraction”.

In summary, the results show a proof-of-concept of the COFB for protein extraction and the potential to transfer the use of COFBs to other bio-based processes that require direct treatment of heterogeneous biomass with high solid content.

References:

[1] Anastas, P. T., & Zimmerman, J. B, Julie B. 2003. „Design Through the 12 Principles of Green Engineering." Anastas, P. T., & Zimmerman, J. B. (2003). Peer Reviewed: Design Through the 12 Principles of Green Engineering. Environmental Science & Technology, 37(5), 94A–101A. Doi:10.1021/Es032373g, 8. https://doi.org/doi:10.1021/es032373g.

[2] Brandi, Francesco. 2022. „Integrierte Bioraffinerie in Kontinuierlichen Fließsystemen Unter Verwendung Nachhaltiger Heterogener KatalysatorenIntegrated Biorefinery in Continuous Flow Systems Using Sustainable Heterogeneous Catalysts". Application/pdf. Universität Potsdam. https://doi.org/10.25932/PUBLISHUP-53766.

[3] Buchmaier, Judith, Sofia Krampl, Manuel Eibinger, Gaurav Singh Kaira, Bernd Nidetzky, und Bettina Muster -Slawitsch. 2024. „Continuous Oscillatory Flow as Process Intensification Strategy in Protein Extraction from Brewer's Spent Grain". Chemical Engineering and Processing - Process Intensification 200 (Juni): 109772. https://doi.org/10.1016/j.cep.2024.109772.

[4] Buchmaier, Judith, Bernd Nidetzky, Bettina Muster, Rama Krishna Gudiminchi, Adam P. Harvey, A. N. Phan, und U. Griesbacher. 2020. „Oscillatory Flow Bioreactor (OFB) Applied in Enzymatic Hydrolysis at High Solid Loadings". Chemical & Biochemical Engineering Quarterly 33 (4): 459–70. https://doi.org/10.15255/CABEQ.2018.1553.

[5] Van Gerven, Tom, und Andrzej Stankiewicz. 2009. „Structure, Energy, Synergy, Time—The Fundamentals of Process Intensification". Industrial & Engineering Chemistry Research 48 (5): 2465–74. https://doi.org/10.1021/ie801501y.

Session 5 – Modeling and Simulation in Engineering / Particle Forum

July 2, 2024 10:30 – 10:50

Lecture Hall i9

Chairperson: Prof. Stefan Radl

10:30

Robot-LDA line measurements on a 30° inclined flat plate in an open wind channel with and without plasma actuation effect

Presenting Author: Manuel Berger

Berger, M[1,*], Wilhelm, M [2], Senfter, T [2], Mayerl C[2] and Pillei, M[2].
[1] Dept. of Medical Technologies, MCI Innsbruck, Austria
[2] Dept. of Industrial Engineering & Management, MCI Innsbruck, Austria
*presenter/corresponding author: manuel.berger@mci.edu

Abstract

Active flow control is a relatively new method to influence the velocity vector field around an airplane wing. Robot-LDA measurements of a 30° inclined flat plate in an open wind channel with and without the local plasma actuation effect are performed. The airflow Reynolds number is approximately 100 000 at a flow rate of 250 m³/h. 44 measurement points in a length of 40 mm orthogonal plate distance are taken. The positions are chosen at 3 mm, 35 mm and 70 mm tangential to the plate tip at plate length of 46 mm. The wind channel axial velocity component without plasma is captured three times. Next, the input voltage and frequency of the plasma actuator were fixed at 14 kV_{p-p} and 5 kHz. Due to stability of the plasma the measurement with local plasma actuation is only repeated two times. Furthermore, due to the plasma ozone is generated during the measurement, which is dangerous for the human body. Results of all five measurement are similar, which means that just with line measurements it is not possible to show the effect of plasma as it shown already by different studies with lower qualitative measurement techniques than Robot-LDA. Next steps are to perform measurements with multiple points on a surface with Robot-LDA, perform PIV measurements or smoke capturing measurements with a camera.

Introduction

The research on active flow control (AFC) began approximately one decade ago due to the fact that dielectric barrier discharge (DBD) actuators were available to generate cold plasma [1,2]. The idea is to use two electrodes with a high voltage sinusoidal wave separated by a layer of dielectric material to prevent the glow-to-arc transition and flush mounted on position of the plate suction surface. This results in an electric or ionic wind with a flow velocity of a few meters per seconds to manipulate the velocity vector field between the two electrodes [3].

In [3] a NACA 4412 airfoil investigation at a Reynolds number of 35 000 was performed. Four different electrode configurations at 10°, 20° and 30° angles of attack were used. For the flow visualization a wind tunnel (TecQipment AF17) with a smoke generator (ViCount Compact 1300) was used. To generate the smoke nontoxic oil is heated up above 300°C to visualize the flow. Photos were taken orthogonal to the flow. For better visualization, 12V LED light strips were placed inside the wind channel. Results show that three of the four electrode configurations have qualitative improvements in separation control (pre-stall, post-stall angles).

Two dimensional, two components (2D, 2C) particle image velocimetry measurements (PIV) were performed in [4,5]. In [4] the DBD was installed on a NACA0015 and investigated at a Reynolds number of 700 000. At the angle of attacks 14.5° and 22° differences in the 2D velocity vector field between on and off plasma source were found. The newest publication, at the time when we started the investigation in 2023, was [5]. A detailed quantitative analysis of the effect of the plasma is performed. Results show a -48% and a -59% position change due to the plasma in the center position of the passage vortex which shows a significant influence. Furthermore, experiments suggests that the installation location of the plasma actuator is before the leading edge of the blade. The higher the Reynolds number the weaker is the vortex suppression effect of the plasma actuator.

In the presented study an own developed ABB RobotStudio® laser Doppler anemometry (LDA) plug-in will be used to position and orient the LDA. Compared to the already existing investigations the LDA features higher temporal resolution and with the robot a higher spatial accuracy than PIV or the smoke investigation. For simplicity, not a NACA profile is investigated but a 30° inclined flat blade with the crosssectional dimensions of 46 mm x 3 mm in an open wind channel with a diameter of 80 mm.

Methods

To perform the LDA measurements a at the MCI developed plugin for RobotStudio® 2021 and ILA LDA control systems qt 2.0.10 was used with the LDA ILA fp50-shifted with the 250 mm lens. The robot was the ABB IRB 1200 7kg 0.7m.

Experimental setup

Within an open wind channel, at a flow rate of 250 m^3/h and a Reynolds number of approximately 100 000, flow investigation on a 30° inclined flat plate with the dimensions of 46 mm x 3 mm are performed. The DBD is mounted as suggested by [5]. The electrode at the top is 5 mm and 15 mm at the bottom with an overlap of 0.5 mm. For both scenarios, either with switched on or switched off DBD experiments are performed. The DBD is powered with a voltage of 14 kV_{p-p} and a frequency of 5 kHz. In total 44 measurements points were taken at three lines, 3 mm, 35 mm and 70 mm tangential to the plate tip at plate length of 46 mm. The velocity component parallel to the wind channel axis is measured by LDA. The LDA parameters are chosen to achieve good signal to noise ratio to detect the particle velocities (sample rate = 50 MHz, Number of samples = 512, Bandpass filter range = 100 kHz – 20 MHz, burst validation factor = 3) with a minimum acquisition time per point of 10 seconds a maximum acquisition time of 30 seconds or a statistical uncertainty < 2%. Seeding droplets consisted of di(2-ethylhexyl) sebacate (DEHS) with a modal diameter of approximately 1.2 µm with a Stokes number smaller than 1 so that the droplets follow the air without any lag.

Preparation 3D-CAD

Initially, the open wind channel with the flat plate is designed in Autodesk Inventor 2022 software, where the origin (x = 0 mm, y = 0 mm, z = 0mm) of the CAD file is the origin of the measurement coordinate system (see Figs. 1 and 2) and saved in ACIS solid modeling format (.sat). The (.sat) file is opened in RobotStudio® 2021. Afterwards, the used robot in laboratory, ABB IRB 1200 7kg 0.7m, is imported and positioned within the CAD. Finally, the LDA is loaded within the software with the tool center point (TCP). One reference frame is generated to define the object coordinate system (see Fig. 1), the same one is also used to define the orientation of the measurement axis. In robotics, there is the definition of a pose, which is at every measurement point a defined position and orientation. For a point measurement the LDA tool TCP must be coincident with the pose.

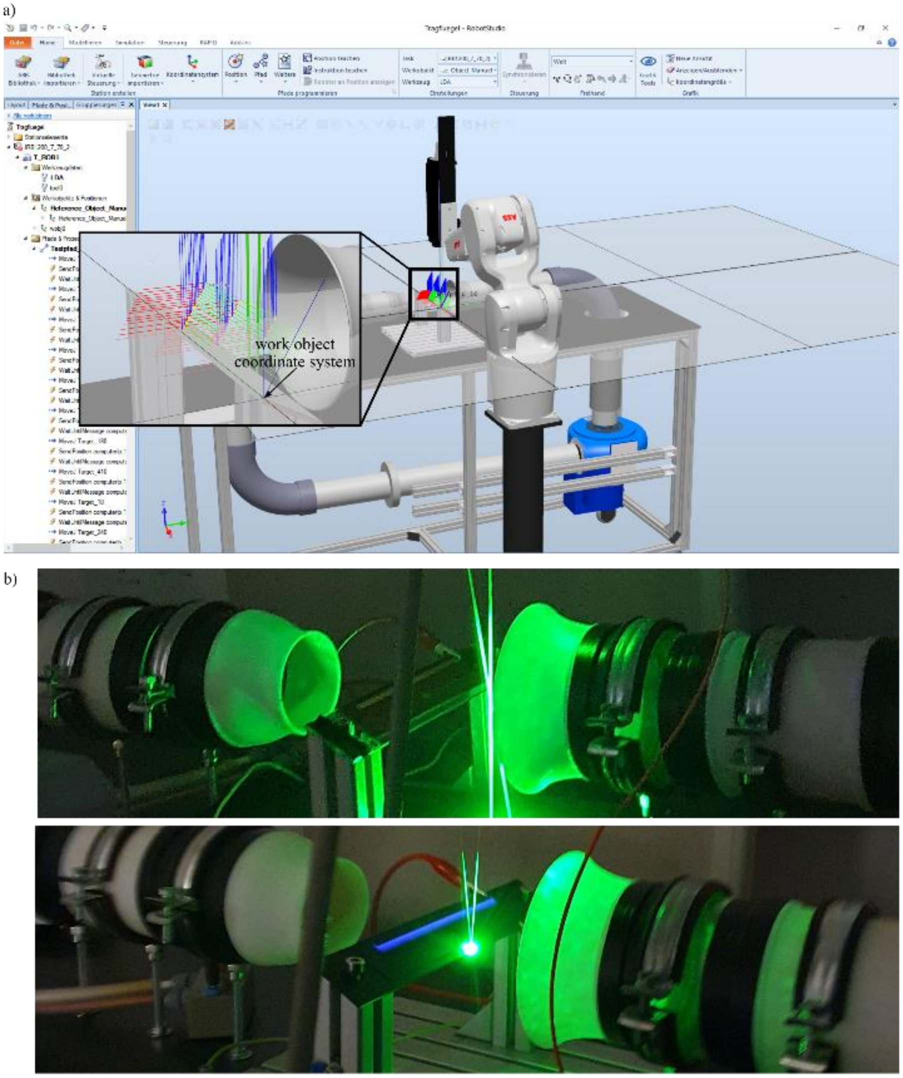

Fig. 1: a) imported CAD of the measurement environment in RobotStudio® with the work object coordinate system used a measurement coordinate system. Furthermore, the LDA tool with the TCP is inserted. Three investigation lines orthogonal to the plate (in total 44 measurement points) are generated. The open wind channel is shown. b) Experimental set up: Robot with LDA measurement, wind channel and plate with switched on and off DBD.

Next, the robot motion for the 44 measurement points are planned. The wind channel axial component is investigated from the top due to best optical accessibility with the robot. The achieve the pose, with the LDA TCP multiple configurations are possible. The configurations are set so that the axes' travel distance between consecutive points is minimal. Therefore, the RobotStudio Auto Configuration path planning option was used. The robot LDA TCP speed was set to 20 mm/s. Simulation of the path planning were performed and send to the robot. The LDA tool is calibrated by jogging (= moving the robot with the Flex Pendant) on one position (a cone) four times with a different orientation. An accuracy smaller than 0.8 mm could be achieved. Subsequently, the work object coordinate system is defined by three points (first one: origin, second one: direction to the x-axis. third one: direction to the y-axis). The z-axis of the work object coordinate system is calculated orthogonally with the two axes.

Postprocessing: Robot-LDA measurement results

The CAD file is saved in stl file format. The measurements in csv file format as well as the measurement results are loaded in ParaView 5.10.1. The imported measurement data is converted to points assigning the spatial coordinates x,y and z. For nice visualization, the transparence level of the open wind channel is set to 47%.

Results and Discussion

Tab. 1 shows the results of the measurement points for all 5 measurements of the 44 measurement points (3 without DBD, 2 with DBD.) N … measurement number, x, y, z … spatial coordinates with respect to the origin (see. Fig. 2), M1,M2, M3 … measurement results without DBD, DBD1, DBD2 … measurement results with DBD. The measurement points 13 – 18 are not valid due to < 50 valid bursts.

N	x	y	z	M1	M2	M3	DBD 1	DBD 2
1	3	140	39	12,01	12,13	12,01	11,71	12,02
2	3	140	38	13,37	13,40	13,37	13,32	13,46
3	3	140	36	14,51	14,42	14,51	14,43	14,44
4	3	140	34	15,12	15,16	15,12	15,11	15,12
5	3	140	31	15,47	15,41	15,47	15,48	15,47
6	3	140	29	15,63	15,54	15,63	15,63	15,60
7	3	140	27	15,64	15,64	15,64	15,72	15,64
8	3	140	24	15,64	15,59	15,64	15,67	15,67
9	3	140	22	15,67	15,60	15,67	15,66	15,62
10	3	140	18	15,55	15,51	15,55	15,61	15,57
11	3	140	16	15,51	15,44	15,51	15,56	15,52
12	3	140	14	15,40	15,35	15,40	15,51	15,43
13	3	140	10	2,86	0,00	2,86	0,00	0,00
14	3	140	5	0,00	0,00	0,00	0,00	0,00
15	3	140	2	31,02	31,02	31,02	0,00	0,00
16	35	140	0	0,00	0,00	0,00	0,00	0,00
17	35	140	1	0,00	5,35	0,00	1,75	5,17
18	35	140	5	0,00	0,00	0,00	0,00	0,00
19	35	140	8	2,51	2,31	2,51	2,20	2,39
20	35	140	10	2,48	2,15	2,48	2,27	2,42
21	35	140	12	2,12	2,24	2,12	2,17	2,31
22	35	140	14	2,22	2,21	2,24	2.14	2,15
23	35	140	16	2,59	2,39	2,59	2,37	2,50

24	**35**	**140**	**19**	**2,95**	**2,84**	**2,95**	**2,74**	**2,75**
25	**35**	**140**	**22**	**2,99**	**2,99**	**2,99**	**2,78**	**2,79**
26	**35**	**140**	**25**	**3,06**	**2,94**	**3,06**	**2,82**	**2,91**
27	**35**	**140**	**28**	**3,22**	**3,15**	**3,22**	**3,08**	**3,15**
28	**35**	**140**	**30**	**4,03**	**4,10**	**4,03**	**4,08**	**3,98**
29	**35**	**140**	**35**	**6,98**	**7,05**	**6,98**	**6,60**	**6,58**
30	**35**	**140**	**39**	**9,99**	**9,76**	**9,99**	**9,71**	**9,65**
31	**70**	**140**	**40**	**2,58**	**2,60**	**2,58**	**2,72**	**2,70**
32	**70**	**140**	**36**	**2,52**	**2,42**	**2,52**	**2,65**	**2,61**
33	**70**	**140**	**34**	**2,54**	**2,54**	**2,54**	**2,68**	**2,65**
34	**70**	**140**	**31**	**2,65**	**2,60**	**2,65**	**2,69**	**2,70**
35	**70**	**140**	**29**	**2,58**	**2,66**	**2,58**	**2,85**	**2,84**
36	**70**	**140**	**27**	**2,71**	**2,73**	**2,71**	**2,89**	**2,78**
37	**70**	**140**	**24**	**2,65**	**2,67**	**2,65**	**2,82**	**2,68**
38	**70**	**140**	**22**	**2,71**	**2,81**	**2,71**	**2,88**	**2,81**
39	**70**	**140**	**18**	**2,64**	**2,64**	**2,64**	**2,64**	**2,71**
40	**70**	**140**	**16**	**2,68**	**2,62**	**2,68**	**2,62**	**2,64**
41	**70**	**140**	**14**	**2,54**	**2,50**	**2,54**	**2,51**	**2,57**
42	**70**	**140**	**10**	**2,76**	**2,73**	**2,76**	**2,75**	**2,73**
43	**70**	**140**	**5**	**4,75**	**4,56**	**4,75**	**4,68**	**4,79**
44	**70**	**140**	**2**	**10,09**	**9,79**	**10,09**	**9,90**	**9,98**

Fig. 2 – Fig. 6 show graphically the LDA measurement results M1, M2, M3, DPD1 and DPD2. The origin (x= 0 mm, y= 0 mm, z= 0 mm) is at the top front corner of the plate. Measurement points are taken in the middle of the plate (y = 140 mm). The color of the points shows the axial velocity component of the wind channel axis measured with the 1D LDA system. Three measurements points at the left row and three in the middle row are not valid.

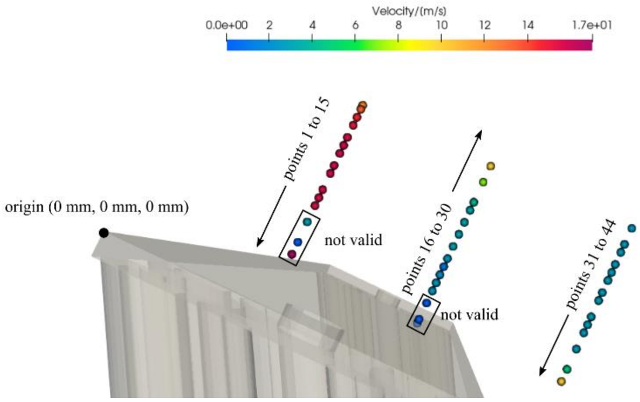

Fig. 2: LDA measurement points M1. ParaView 5.10.1 is used for post processing. STL file is loaded with 47% transparency. Point color shows the wind channel axial component. Switched off DBD.

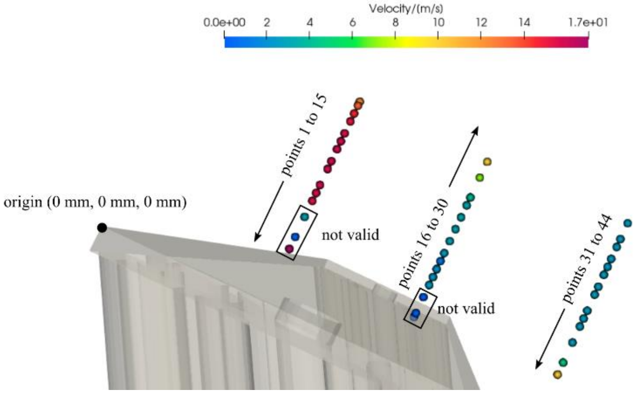

Fig. 3: LDA measurement points M2. ParaView 5.10.1 is used for post processing. STL file is loaded with 47% transparency. Point color shows the wind channel axial component. Switched off DBD.

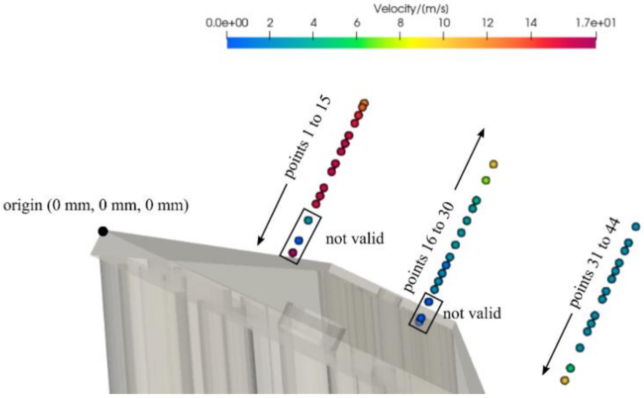

Fig. 4: LDA measurement points M3. ParaView 5.10.1 is used for post processing. STL file is loaded with 47% transparency. Point color shows the wind channel axial component. Switched off DBD.

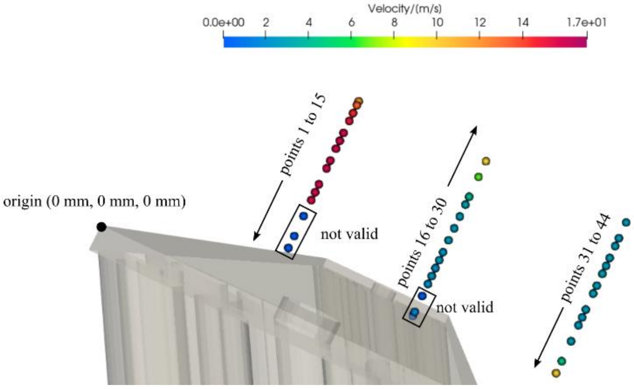

Fig. 5: LDA measurement points DBD 1. ParaView 5.10.1 is used for post processing. STL file is loaded with 47% transparency. Point color shows the wind channel axial component. Switched on DBD.

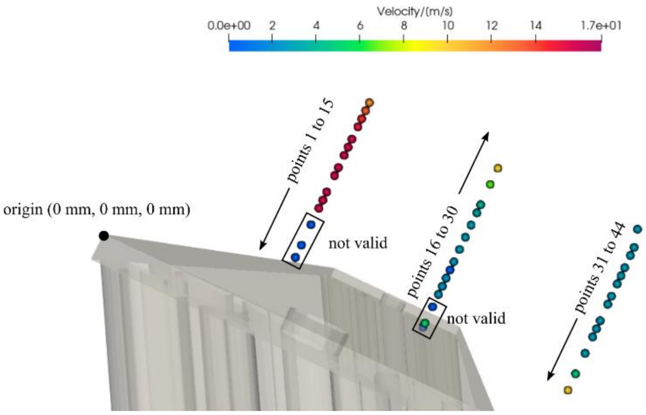

Fig. 6: LDA measurement points DBD 2. ParaView 5.10.1 is used for post processing. STL file is loaded with 47% transparency. Point color shows the wind channel axial component. Switched on DBD

In the results (Fig. 2 to Fig. 6) there is a not constant spatial resolution at the measurement points set. This is due to the fact the for point planning RobotStudio is used. In RobotStudio there is a point creation tool for surfaces and volumes. For the presented study a very thin (1mm) surface in y-direction is created with the spatial dimension in z-axis. Furthermore, the point numbers (1-44) are structured in a way that the robot has limited amount of distance for the movement from one point to the next point. Therefore, the first row starts from the top left (see Fig. 2), continues until the laser crossing point intersects with the flat plat. Then results of middle row are determined from bottom to top and at right row again from top to bottom. All results show a higher velocity outside the shadow region of the flat plate. At a investigated flow rate of 250 m³/h this results in a free-stream velocity $\boldsymbol{u}_\infty$ = 15 m/s. The more the measurement point is in the shadow region (closer to the wall) the smaller the velocity will get. Due to laser beam reflections from the wall (see Fig. 1b) or less seading withing the shadow region, 6 measurement points at each setup (M1 & M2 & M3 & DBD1 & DBD2) are not valid. For a valid signal at least 50 valid LDA measurement bursts are defined. For all other measurement points more than 1000 valid bursts were found.

All five measurements, with and without DBD, shows similar results (see Tab. 1), which means for the set of points, the plasma has no influence on the velocity component (wind channel axial component).

Acknowledgements

We thank Thomas Hausberger and Johannes Sieberer for developing the ABB-Robot LDA plugin within their master theses.

References:

[1] E. Moreau, Airflow control by non-thermal plasma actuators, J. Phys. D. Appl. Phys. 40 (2007) 605.

[2] N. Benard, E. Moreau, Electrical and mechanical characteristics of surface AC dielectric barrier discharge plasma actuators applied to airflow control, Exp. Fluids 55 (2014) 1–43.

[3] B. Karadag, C. Kolbakir, A.S. Durna, Plasma actuation effect on a NACA 4412 airfoil, Aircr. Eng. Aerosp. Technol. 93 (2021) 1610–1615.

[4] G. Zoppini, M. Belan, A. Zanotti, L. Di Vinci, G. Campanardi, Stall control by plasma

actuators: Characterization along the airfoil span, Energies 13 (2020) 1374.

[5] T. Matsunuma, Effects of the installation location of a dielectric barrier discharge plasma actuator on the active passage vortex control of a turbine cascade at low Reynolds numbers, in: Actuators, MDPI, 2022: p. 129.

10:50

Application of a novel hybrid multi-scale model in a fluidized bed with an immersed tube

Presenting Author: Behrad Esgandari

Behrad Esgandari.[1,*], Simon Schneiderbauer [1]
[1] Department of Particulate Flow Modelling, Johannes Kepler University Linz (JKU), Austria
*presenter/corresponding author: behrad.esgandari@jku.at

Abstract

We present a novel hybrid multi-scale model, referred to as the "discrete magnification lens" method, that employs a computational fluid dynamic coupled to discrete element method (CFD-DEM) approach within a specific region of interest in a two-fluid model (TFM) simulation. This model combines the advantages of both TFM and CFD-DEM approaches, while maintaining computational speed and accuracy. This model can be plugged into a TFM model and used to calculate the properties based on Lagrangian data. We applied the discrete magnification lens (DML) to a fluidized bed with an immersed tube to evaluate the erosion of the tube caused by the particle impacts. It was found that the DML model is capable of improving the accuracy of the TFM compared to the CFD-DEM, while requiring less computational time than the CFD-DEM.

Introduction

Particle-laden flows are prevalent in many engineering applications, including, pneumatic conveying, and fluidized beds. Three common approaches to simulate fluid-particle systems are: particle-resolved direct numerical simulation (PR-DNS), Euler-Lagrange models (e.g., unresolved CFD-DEM or CFD-DEM), and Euler-Euler models (e.g., TFM) [1]. The PR-DNS method is the most detailed method to model particle-laden flows, since it can resolve all the time and length scales of both phases. In the CFD-DEM the particles are tracked individually while the fluid is modelled using a gird larger than particle diameter, while both fluid and particle phases are treated as continuum phases in the TFM. In addition to use of the same volume-averaged Navier-Stokes equations to model the fluid phase, the same interphase force closures are used to achieve the interphase coupling in the TFM and the CFD-DEM approaches.

The similarities between the TFM and the CFD-DEM approaches has led to the development of new hybrid multi-scale methods. These models attempt to leverage the lower computational requirements of the less accurate model and the accuracy of the detailed models at the same time. These concurrent hybrid multi-scale models are classified into two categories: (1) those that use a ”shared domain” approach, where both models are existing in the whole simulation domain, and (2) those that use a ”domain decomposition” approach, where the detailed model is only applied in a small sub-domain to improve the predictions of the less detailed model.

In this study, we introduce a novel hybrid multi-scale modeling approach referred to as “discrete magnification lens” (DML) model based on “domain decomposition” approach. First, both individual approaches are validated against experimental data. Then, we apply the DML model to a fluidized bed with an immersed tube to calculate the erosion of the tube caused by particle impacts. Also, the time-averaged profiles of particle volume fraction and vertical particle velocities are compared between the TFM, the CFD-DEM and the DML approaches.

Methodology

The locally averaged mass and momentum equations for the fluid and the continuum particle phases in the TFM are written as,

$$\frac{\partial}{\partial t}\left(\alpha_q\rho_q\right) + \nabla\cdot\left(\alpha_q\rho_q\mathbf{u}_q\right) = 0 \tag{1}$$

$$\frac{\partial}{\partial t}\left(\alpha_f\rho_f\mathbf{u}_f\right) + \nabla\cdot\left(\alpha_f\rho_f\mathbf{u}_f\mathbf{u}_f\right) = -\alpha_f\nabla p + \nabla\cdot\alpha_f\tau_f - \beta_{TFM}\left(\mathbf{u}_f - \mathbf{u}_{cp}\right) + \alpha_f\rho_f g \tag{2}$$

$$\begin{aligned}\frac{\partial}{\partial t}\left(\alpha_{cp}\rho_{cp}\mathbf{u}_{cp}\right) + \nabla\cdot\left(\alpha_{cp}\rho_{cp}\mathbf{u}_{cp}\mathbf{u}_{cp}\right) = &- \alpha_{cp}\nabla p - \nabla\cdot\left(S^{kc}_{cp} + S^{fr}_{cp}\right) + \beta_{TFM}\left(\mathbf{u}_f - \mathbf{u}_{cp}\right)\\ &+ \alpha_{cp}\rho_{cp} g + \mathbf{\Psi}_{cp}\end{aligned} \tag{3}$$

where in Eq. (1), $\mathbf{u_q}$, α_q and ρ_q are the velocity, volume fraction and density of phase q, where q represents either the particle phase or fluid phase. In addition, β_{TFM} is the drag coefficient in TFM simulations where the drag model of Beetstra et al. [2] is used in this study. It can be noted that in equation (3) solids stress tensor consists of kinetic-collisional, S^{kc}_{cp}, and frictional solids stresses, S^{fr}_{cp}. The variable $\mathbf{\Psi}_{cp}$ in Eq. (3) denotes a semi-implicit source term used in DML and will be discussed later. Moreover, for detailed explanations about the TFM constitutive relations, we refer to our previous paper [3]. Note that we do not discuss the equations related to the CFD-DEM approach in here, the interested reader is referred to our previous paper [3].

In the DML, the CFD-DEM is nested into a TFM simulation. In other words, the CFD-DEM acts like a magnification lens and magnifies the continuum particle phase by using the discrete particles in a specific region of interest. The schematic of the DML is illustrated in Fig. 1. The region indicated with the cyan color represents a TFM simulation and the region in the left-hand side of the overlapping boundary marked by the green color is the CFD-DEM domain. It can be deduced that the DML region is composed from different parts.

The *overlapping boundary* is the shared boundary between the TFM and the CFD-DEM domains. This boundary is utilized to quantify the inflow mass flux of the continuum particle phase into the CFD-DEM at each cell face. The number of discrete particles to be inserted into the CFD-DEM domain can be determined by utilizing the measured mass flux of the continuum particle phase at the cell faces. The *insertion region,* represents the region where the discrete particles are inserted. This region consists of the initial layer of cells that are located near the overlapping boundary. The initial velocity vector of the newly inserted discrete particles can be assigned by randomly sampling from the Maxwellian velocity distribution. In the *particle velocity controller region,* the deviation of the velocity of discrete particles compared to the continuum particle phase velocity in the cell corresponding to the particle's position is minimized. The velocity of discrete particles is controlled by adding a force on every discrete particle in the particle velocity controller region. This force is defined as,

$$\mathbf{F}_{\text{controller},i} = \boldsymbol{\rho}_{dp}\boldsymbol{V}_{dp}\left(\left[\mathbf{u}_{cp}\right]_{@i} - \left[\overline{\mathbf{u}_{dp}}\right]_{@i}\right)/\boldsymbol{\Delta t}_{\text{coupling}} \tag{4}$$

where $\overline{\mathbf{u}_{dp}}$ is the mapped and smoothed discrete particle velocity. $[\quad]_{@i}$ indicates the interpolation of the value to the position of the particle using a trilinear interpolation method and $\boldsymbol{\Delta t}_{\text{coupling}}$ is the coupling time step between the TFM and the CFD-DEM. The *relaxation region* is used to dampen the possible disturbances on the discrete particles caused by the imposed forces on the particles. In the *two-way coupling region,* the discrete particles' information is used to influence the underlying TFM simulation, resulting in a two-way coupling between the TFM and the CFD-DEM models. To do so, a semi-implicit source term, $\boldsymbol{\Psi_{cp}}$, is added to the RHS of Eq. (3) which pushes the continuum particle phase velocity of the underlying TFM towards the discrete particle velocity field. This term is described as,

$$\boldsymbol{\Psi_{cp}} = \boldsymbol{\alpha_{cp}\rho_{cp}}\left(\mathbf{u}_{cp}^{n+1} - \overline{\mathbf{u}_{dp}}^{n}\right)/\boldsymbol{\Delta t}_{\textbf{coupling}} \tag{5}$$

Where $n+1$ shows the implicit term while n is the explicit one. In addition to $\boldsymbol{\Psi_{cp}}$, the interphase momentum exchange coefficient of the continuum particle and fluid phases, β_{TFM}, in Eq. (2)-(3), is replaced by the interphase momentum exchange coefficient obtained from the CFD-DEM simulations.

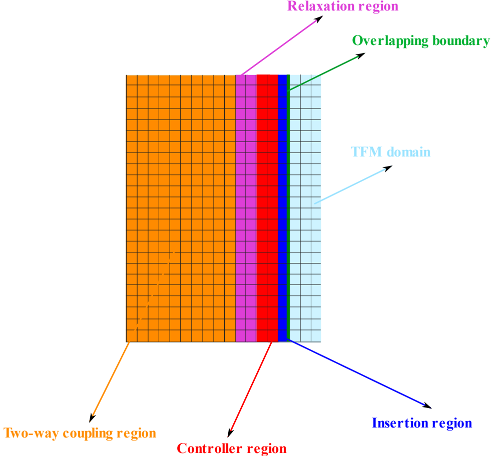

Fig. 1 The schematic of the DML model.

Results

The fluidized bed set-up used for simulations is based on the experimental work of Zhou and Zhao [4] and shown in Fig. 2(a). Initially the bed contains 332000 particles with dimeter of 0.0015 m and density of 2576 kg/m^3. The information about the simulation parameters can be found in Zhou and Zhao [4]. The TFM and the CFD-DEM approaches are validated against the experimental time-averaged pressure drop values at different superficial fluid velocities and shown in Fig. 2(b). It can be seen that with increasing the superficial fluid velocity, the pressure drop increases till minimum fluidization point where the pressure drop balances the bed weight. Both simulation approaches can predict this trend in a good agreement with experiments.

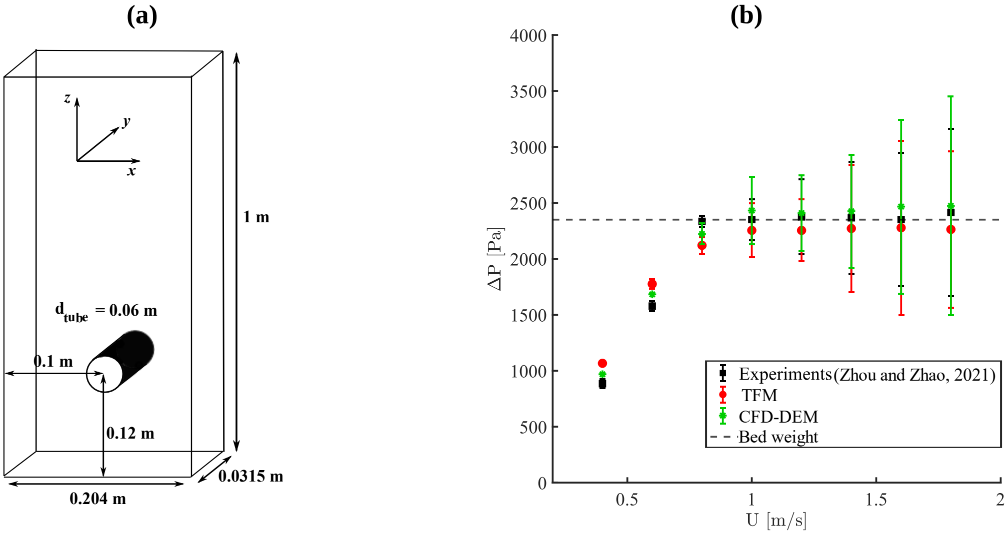

Fig. 2 (a) The schematic of the fluidized bed. (b) Comparison of time-averaged pressure drop between the experiments and simulations at different superficial velocity.

It is not possible to calculate the erosion on the immersed tube using the TFM, because it requires the information about the particle-wall contacts. However, it is feasible to obtain such data from the CFD-DEM simulations using the shear impact energy model (SIEM) [5]. The DML model can equip the TFM with the ability to calculate the erosion on the tube, if the DML region is placed around the tube. Therefore, we place the DML region from x = -0.066 to x = 0.066, and from z = 0.054 m to z = 0.186 m, while it covers depth of the bed. We define four particle controller cells in left, right, top and bottom of the DML region, and the two-way coupling region spans from x = -0.048 m to x = 0.048 m, and from z = 0.072 m to z = 0.168 m covering depth of the bed. Fig. 3 (a)-(b) shows the time-averaged particle volume fraction and vertical particle velocities at z = 0.15 m. It can be deduced that applying the DML method improves the accuracy of the results of the TFM in terms of time-averaged quantities such as particle volume fraction and vertical particle velocities compared to the CFD-DEM. The relative root mean square error of the time-averaged particle volume fraction for the TFM is 9.95%. However, when the DML model is applied, the error decreases to 8.4%. Moreover, it can be seen from Fig. 3 (c) that it is possible to predict the erosion on the immersed tube from the TFM by means of the DML model with a good agreement with the data from the CFD-DEM. Furthermore, the DML model simulation was three times faster than the CFD-DEM, whereas it needed more computational time comparted to the TFM.

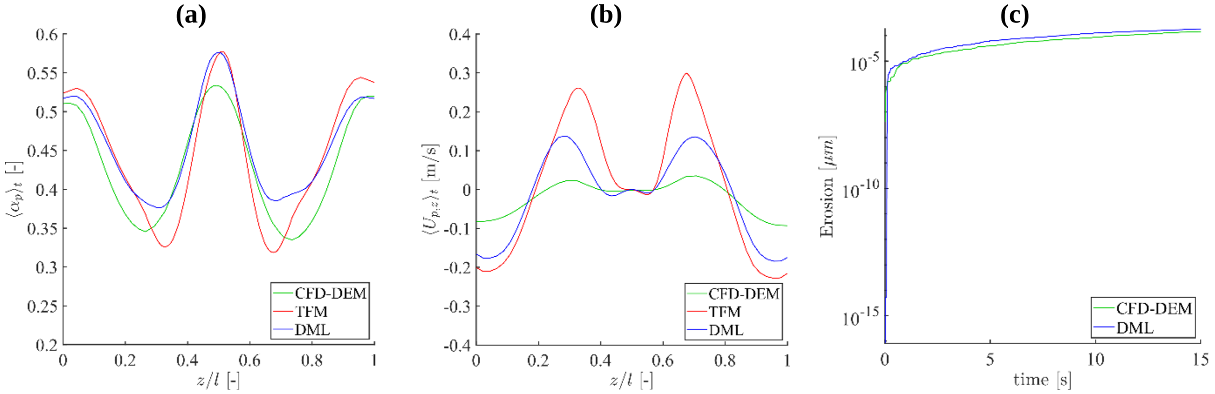

Fig. 3 (a) Time-averaged particle volume fraction. (b) Time-averaged vertical particle velocities. (c) Erosion of the tube with time.

Conclusions

We implemented a discrete magnification lens model for simulations of fluidized beds. It was shown that it is able to augment the TFM with Lagrangian data in the region of interest, which for example can be useful in evaluating erosion on an immersed tube. Also, it was found that the DML is capable of improving the results of the TFM compared to the CFD-DEM. In addition, the DML model requires less computational time than the CFD-DEM.

References:

[1] S. Subramaniam and S. Balachandar, “Modeling Approaches and Computational Methods for Particle-laden Turbulent Flows,” 2023.

[2] R. Beetstra, M. A. Van Der Hoef, and J. A. M. Kuipers, “Drag force of intermediate reynolds number flow past mono- And bidisperse arrays of spheres,” *AIChE Journal*, vol. 53, no. 2, pp. 489–501, 2007, doi: 10.1002/aic.11065.

[3] B. Esgandari, S. Rauchenzauner, C. Goniva, P. Kieckhefen, and S. Schneiderbauer, “A comprehensive comparison of Two-Fluid Model, Discrete Element Method and experiments for the simulation of single- and multiple-spout fluidized beds,” *Chem Eng Sci*, vol. 267, 2023, doi: 10.1016/j.ces.2022.118357.

[4] L. Zhou and Y. Zhao, “CFD-DEM simulation of fluidized bed with an immersed tube using a coarse-grain model,” *Chem Eng Sci*, vol. 231, Feb. 2021, doi: 10.1016/j.ces.2020.116290.

[5] H. Ashrafizadeh and F. Ashrafizadeh, “A numerical 3D simulation for prediction of wear caused by solid particle impact,” *Wear*, vol. 276–277, pp. 75–84, Feb. 2012, doi: 10.1016/j.wear.2011.12.003.

11:10

A Random Forest modeling approach for packed column hydraulics

Presenting Author: Marcus Schlager

Schlager, M.[1,2,*], Tippayawong, N. [2], Wolf-Zöllner, V.[1]
[1] Montanuniversität Leoben, Franz Josef-Straße 18, 8700 Leoben
[2] Chiang Mai University, 239 Huay Kaew Rd., Chiang Mai 50200, Thailand
*presenter/corresponding author: marcus.schlager@unileoben.ac.at

1. Introduction

Accurate prediction of gas-side pressure drop and liquid holdup in packed distillation or absorption columns is essential for apparatus dimensioning. As a results, many semi-empirical models such as Stichlmaier et al. (1989), Billet and Schultes (1991) or Maćkowiak (2010) have been developed. The main drawback of these modeling approaches is that they typically rely on one or more experimentally determined packing-specific parameters that must be obtained through measurements before being able to describe a packing.

The objective of this research is to derive a regression model for structured column packing pressure drop and liquid holdup that fully eliminates the need for packing-specific model parameters. Once such a model is trained, packing hydraulics can be predicted directly from packing descriptors. In particular, the proposed model could be used to calculate hydraulics of novel packing geometries, without first having to characterize such geometries experimentally.

2. Modeling approach

Random Forest (Figure 6 left) is an ensemble learning approach from the domain of machine learning. The Random Forest is constructed from a large number of randomized decision trees. To avoid overfitting, each decision tree is trained on only a random subset of the data and only considers a random subset of model features (a process called bootstrap aggregating). To arrive at an overall model prediction, the predictions of the individual decision trees are averaged. During model fit, the individual decision trees are created. The overall behavior of the algorithm can additionally be controlled through so-called model hyperparameters, e.g. the total number of trees or the maximum depth of an individual tree. Random Forest is versatile, has shown excellent performance in many settings and returns measures of variable importance for model interpretability (Biau and Scornet, 2016). The Random Forest regression model is trained using the sklearn library (Pedregosa et al. 2011) for the Python programming language.

The modeling workflow starts with splitting the data into two sets: a training set (80% of measurements) and a test set (20% of measurements). Model hyperparameters are determined by simulating a validation set through 5-fold cross-validation on the test set (Figure 6 right). After optimal hyperparameters are obtained, the model is trained using the entire training set. Next, model performance is evaluated on the test set, to ensure model generalizability to data not seen during model training. If the model achieves satisfactory performance, it undergoes a final retraining on the entire data (training and test data).

The following packing properties are chosen as model features: packing porosity, specific geometric area, packing angle, channel side length, channel angle, and free surface area. A total of 6 packing properties are therefore considered as model features.

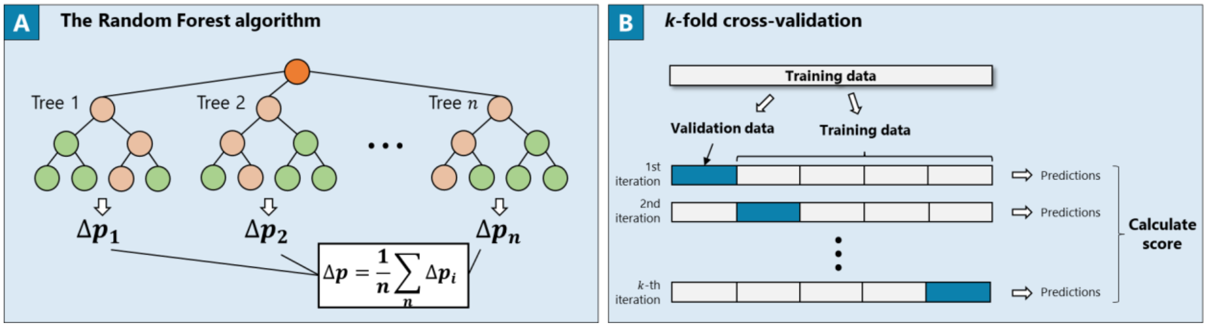

Figure 6. Schematic illustration of the Random Forest regression model and the cross-validation strategy. A) Random Forest is an ensemble model composed of individual decision trees. B) For model hyperparameter calculation the training data is randomly split using *k*-fold cross-validation, with parts of the data used as training data and the remaining data used as validation data during each iteration.

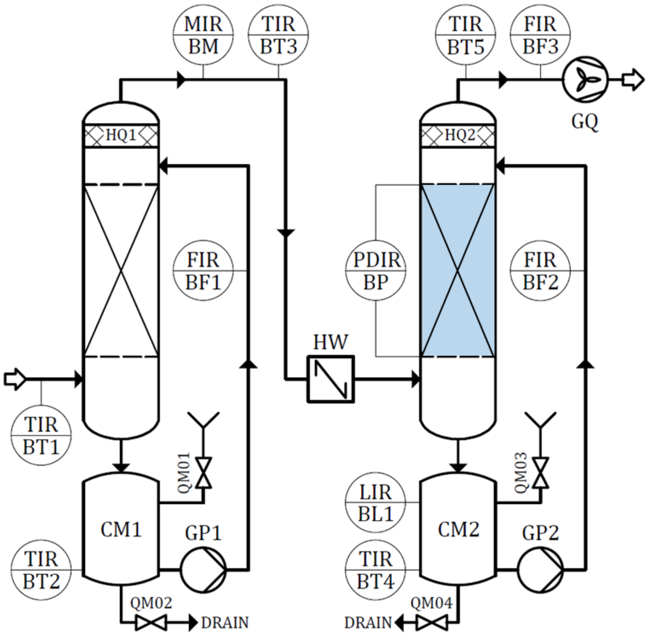

Figure 2. Experimental apparatus for the determination of packed column hydraulics. Left: Saturator column. Right: Measurement column.

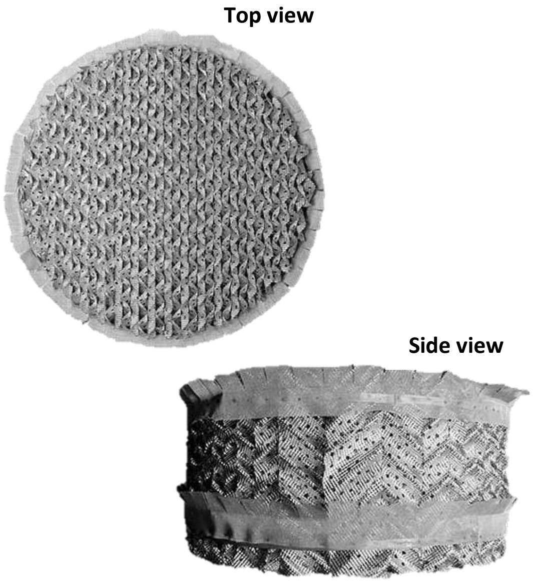

Figure 3. Individual segment of the RMP N 250Y packing, diameter 420 mm) equipped with wall wipers. The packing angle of 45° is recognizable from the side view.

3. Experimental

The experimental apparatus for packing hydraulics characterization (Fig. 2) consists of a saturator column (600 mm) and a measurement column (422 mm) manufactured from polypropylene. Measurements are conducted using the air/water system at ambient temperature and pressure. The apparatus is described in detail in Schlager et al. (2022).

The apparatus operates as follows: First, ambient air is introduced into the saturator column and contacted with deionized water. After exiting the saturator column through a demister mesh, gas phase relative humidity is over 90%, ensuring that no significant amount of liquid phase evaporates in the measurement column. Next, the gas phase flows into the measurement column at the bottom side and flows vertically upwards through the column packing under investigation (maximum packing height up to 2 m).

For pressure drop determination, liquid load in the measurement column is first set to a constant value between 10 and 100 m³/(m²h). Next, the lowest gas load of approx. F=0.5 Pa$^{0.5}$ is set. After reaching stationary conditions, pressure drop is determined using a differential pressure gauge with measuring points above and below the column packing. Gas load is then incrementally increased to repeat the pressure drop measurement procedure at multiple gas loads. A measurement series is concluded after packing flooding or after a maximum gas load of F=5 Pa$^{0.5}$ is reached. The measurements are repeated at different liquid loads.

To measure liquid holdup, the liquid level inside tank CM2 is determined before the start of each measurement series. During experiments, the liquid level inside the tank reduces due to liquid holdup inside the column packing. From this, liquid holdup is calculated using a volume balance.

As of now, 21 structured column packings are investigated in this study. As an example, the RMP N 250Y packing is depicted in Fig. 3. This packing has a geometric area of 250 m²/m³ and a packing angle of 45°. Although most of the examined column packings are commercially available products, some were specially manufactured for this study. For example, the data set includes packings with packing angles of up to 80°. As a result, the validity range of the derived model is increased.

4. Results

Random Forest regression model predictions for pressure drop and liquid holdup are given in Fig. 4. A total of 1714 individual measurements were available for pressure drop modeling while a total of 1455 individual measurements were available for liquid holdup modeling.

After hyperparameter tuning, the regression model is found to give good fit for both pressure drop (R^2=0.98) and liquid holdup (R^2=0.87) on the training data.

Model generalizability (judged through model predictions of test data) is quite satisfactory. Pressure drop (R^2=0.81) is reproduced particularly well for lower pressure drop of up to 500 Pa/m. In this region, most model predictions lie within 20% of the corresponding measurements. Above 500 Pa/m, model predictions start to increasingly scatter and the model slightly underpredicts pressure drop starting at about 1000 Pa/m. Considering liquid holdup (R^2=0.83), slightly larger deviations between model predictions and measurements exist in the region of low holdup up to approx. 0.15 m³/m³, but overall model predictions are in very good agreement with measured values for the entire range.

5. Conclusions and Outlook

Taken together, the Random Forest modeling approach is found to already give good model fit and generalizability for both pressure drop and liquid holdup. The regression model is already a serious contender of established semi-empirical modeling approaches for packing hydraulics without requiring packing-specific constants.

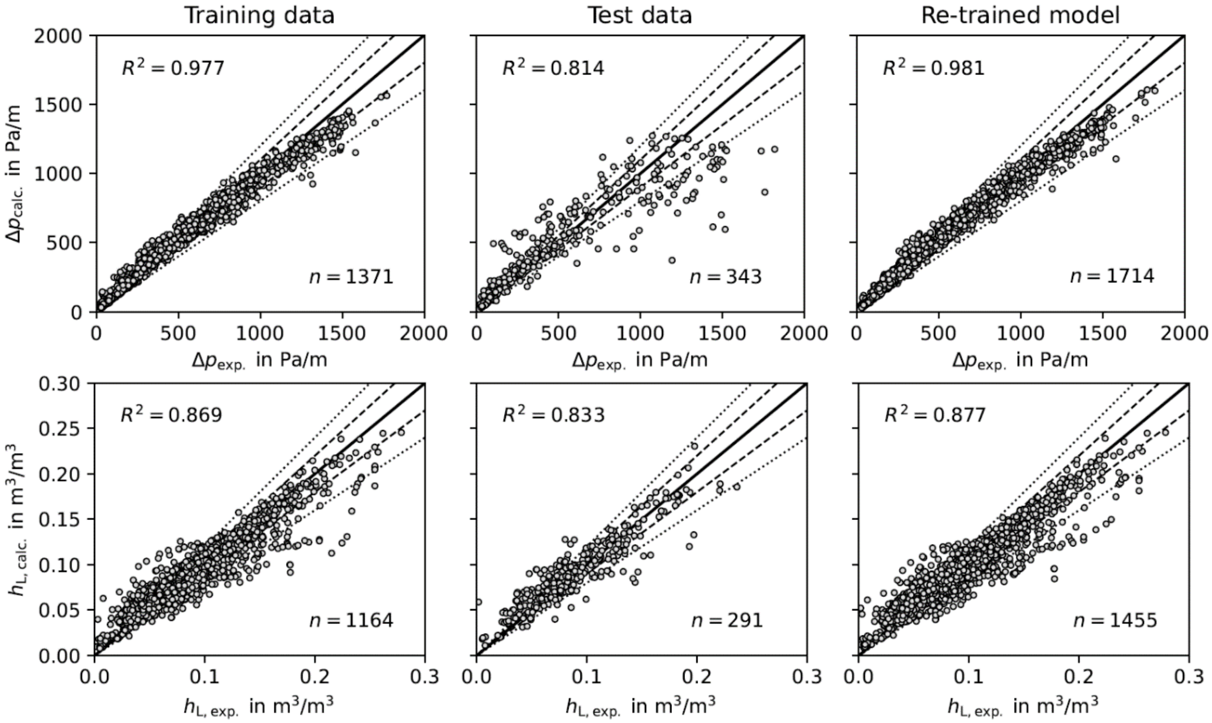

Figure 7. Packed column hydraulics modeling results. Top row: pressure drop; bottom row: liquid holdup. First, model parameters and hyperparameters are calculated from training data (left column). Next, model generalizability is confirmed from test data (middle column). Finally, the model is retrained using the entire data set (right column). Dashed lines: ±10%, dotted lines: ±20%.

Further steps include improvement of model accuracy and generalizability by considering measurement data of additional packings. Additionally, model hyperparameter tuning may further improve model generalizability. In addition to Random Forest, the suitability of other regression models (e.g. gradient boosting) for this application will be investigated.

Acknowledgement. This work has received funding through the research project "SME 5.0 – A Strategic Roadmap Towards the Next Level of Intelligent, Sustainable and Human-Centred SMEs" funded in the European Union's Horizon MSCA 2021 programme under the Marie Skłodowska-Curie grant agreement No. 10108648.

References:

[1] Stichlmair, J., Bravo, J.L., Fair, J.R. (1989), "*General model for prediction of pressure drop and capacity of countercurrent gas/liquid packed columns*," Gas Separation & Purification 3.

[2] Billet, R., Schultes, M. (1991), "*Modelling of pressure drop in packed columns*," Chemical Engineering & Technology 14.

[3] Maćkowiak, J. (2010), "*Fluid dynamics of packed columns*," Springer Berlin Heidelberg.

[4] Pedregosa, F., Varoquaux, G., Gramfort, A. et al. (2011), "*Scikit-learn: Machine Learning in Python*," Journal of Machine Learning Research 12.

[5] Biau, G., Scornet, E. (2016), "*A random forest guided tour*," TEST 25.

[6] Schlager, M., Haushofer, G., Triebl, A., Wolf-Zöllner, V., Lehner, M. (2022), „*Determination of volumetric mass transfer coefficients of structured packings at two different column diameters*," Chemical Engineering Research and Design 186.

11:30

Discrete Modeling of Interlocking and Cohesive Bulk Solids using Tetrapods

Presenting Author: Stefan Radl

Radl, S.[1,*], Mitterlindner, M. [1], and Maier, L. [1]
[1] TU Graz, Institute of Process and Particle engineering, Inffeldgasse 13/III, 8010 Graz
*presenter/corresponding author: radl@tugraz.at

The simulation of poorly flowing (i.e., cohesive and strongly interlocking) bulk solids will play a crucial role in the near future, providing pathways towards efficient utilization of valuable resources and mitigation of environmental impacts. Biomass utilization and different recycling processes, e.g., for batteries or polymers, are examples for these developments. Our present contribution focuses on simulating the handling of shredded nickel-metal hydride (Ni-MH) batteries during a typical recycling process: after a shredding step, the material must be conveyed and cooled prior to storage. The modeling process is challenging due to (i) the cohesive nature of the material (mainly caused by interlocking flakes, fine particles, and liquid bridges), (ii) large differences in the material behavior when stress is applied (ranging from low stress flow to high pressure compaction), and (iii) the low effective heat conductivity of the material. To address these challenges, we propose a novel parcel-based DEM approach [1, 2] using tetrahedral multi-spheres (i.e., “tetrapods”). Specifically, three key improvements were implemented in the tool LIGGGHTS [3]:
(1) Finite intra-tetrapod heat conduction: this feature overcomes the unphysical infinite heat rate transfer problem present in the classical multi-sphere approach. Our "intra multi-sphere thermal conductivity" model predicts the exchanged heat between individual spheres that constitute the tetrapod. By adjusting this conductivity value, heat transfer within a tetrapod can be tuned to better reflect the presence of air gaps and match the effective bulk conductivity of a granular material.
(2) Flexible tetrapods: this feature allows individual spheres within a tetrapod to displace towards the center of mass. While rigid tetrapods (i.e., the vanilla multi-sphere implementation) with a simple cohesion model already perform well in low stress scenarios (e.g., a draw-down test), a compaction process requires flexible tetrapods.
(3) Distributed contact force parameters: next to a mean value (e.g., for friction or cohesion strength), our implementation allows us to consider the contact-to-contact variability of such any contact force parameter.

References:

[1] S. Radl, C. Radeke, J. G. Khinast, and S. Sundaresan, “Parcel-Based Approach For The Simulation Of Gas-Particle Flows,” 8th Interantional Conf. CFD Oil Gas, Metall. Process Ind., no. June, pp. 1–10, 2011.

[2] J. Tausendschön, J. Kolehmainen, S. Sundaresan, and S. Radl, “Coarse graining Euler-Lagrange simulations of cohesive particle fluidization,” Powder Technol., vol. 364, pp. 167–182, 2020, doi: 10.1016/j.powtec.2020.01.056.

[3] C. Kloss, C. Goniva, A. Hager, S. Amberger, and S. Pirker, “Models, algorithms and validation for opensource DEM and CFD-DEM,” Prog. Comput. Fluid Dyn., vol. 12, no. 2–3, pp. 140–152, 2012, doi: 10.1504/PCFD.2012.047457.

Session 6 – Advancements in Gas Processing and Biomass Gasification Technologies

July 2, 2024 10:30 – 10:50

Lecture Hall i8

Chairperson: Prof. Gernot Krammer

10:30

Design of gas disperser for power to gas processes in bubble columns

Presenting Author: Florian Klapal

F. Klapal [1,*], M. W. Hlawitschka [1]
[1]Johannes Kepler University, Institute of Process Engineering, Altenberger Str. 69, 4040 Linz, Austria;
tel. +43 732 2468 9751, email: florian.klapal@jku.at

Power-to-gas technology aims to cost-effectively and efficiently store renewable energy in the gas grid for a longer period of time, while transitioning to a climate-neutral gas grid. Methane with its high calorific value (36 MJ m^{-3}), serves as a promising candidate for this process, doubling as a fundamental chemical for industrial applications. Catalytic methanation stands as a well-established method for this conversion; however, its reliance on high reaction temperatures (200 to 400°C) and expensive metal catalysts render it energy-intensive and economically burdensome. An emerging alternative is biological methanation utilizing archaea, enabling operation at lower temperatures (50 to 60°C). Additionally, the adoption of bubble columns over continuous stirred tank reactors presents another energy-saving improvement.

Bubble columns do not require stirrers to achieve sufficient mixing, as the gas introduced through the disperser system provides the necessary hydrodynamic mixing. The initial formation of bubbles is influenced by various physical parameters, such as density, viscosity and surface tension. Coalescence effects occur after the gas leaves the disperser, which can further affect the size and shape of the bubbles. While certain parameters are primarily dictated by the reaction, the design of the disperser can strongly influence bubble formation, subsequent hydrodynamics and mass transfer efficiency.

To capitalize on the strengths of pipe and plate dispersers, we developed our own disperser type. Its head resembles that of a plate disperser, allowing for customizable pore arrangements. Below the head, a cone-shaped gas chambre connects to a pipe for gas supply, facilitating swift installation. This unique design inspired the name ‘Plug-In’ disperser. For comparison a plate disperser and two porous pin dispersers were also investigated.

To assess the effectiveness of the dispersers, various parameters were studied. The average bubble diameter and deviation were determined by incrementally increasing the gas flow rate and recording the bubble behaviour with a high-speed camera. Images were analysed using different types of bubble detection software and the resulting hydrodynamics were interpreted. Additionally, the total gas holdup was determined by measuring the height of the increasing surface levels in relation to the gas flow rate.

Furthermore, mass transfer efficiency was assessed by introducing carbon dioxide into a sodium hydroxide solution and recording the resulting pH change.

The obtained results demonstrate that altering the disperser design can influence parameters such as the average bubble diameter, the total gas holdup or reaction time. We have shown that while the average bubble diameter significantly affects mass transfer, achieving smaller bubbles alone does not guarantee a rapid reaction due to their limited mixing capability. Further investigation into this topic is essential for enhancing bioprocesses in columns as opposed to agitated tanks.

10:50

Load-flexible biogas methanation in a cooled tube reactor

Presenting Author: Katrin Salbrechter

Salbrechter, K.[1,*], Krammer, A. [1], Lehner, M. [1].
[1] Chair of Process Technology and Environmental Engineering, Montanuniversität Leoben, Franz-Josef Straße 18, 8700 Leoben, Austria
*Presenter/corresponding author: Katrin.salbrechter@unileoben.ac.at

1. Introduction

In the pursuit of sustainable energy, the incorporation of renewable biomethane into current energy systems is essential. With regulations pushing for more biomethane usage, there's a growing demand for efficient and scalable methods to produce it. While fixed bed reactors are commonly used for catalytic methanation because of their simplicity and scalability, they face challenges due to their inherent thermodynamic limitations. Overcoming these limitations is crucial to ensure these reactors perform optimally and efficiently. In this paper, a specific tube-in-tube reactor design is evaluated on how the combination of gas hourly space velocity and the cooling temperature affects the operating window of a single-stage methanation process. The aim is to experimentally determine the load flexible operation range using gas hourly space velocity variation.

2. Description of the reactor set-up

At the Chair of Process Technology at Montanuniversität Leoben, an actively cooled tube-in-tube reactor for catalytic methanation has been developed. High gas velocities and turbulences in the tube reactor improve the radial heat transport and allow operation scenarios with a high load flexibility.
The reactor design and the installed cooling system are evaluated in a small laboratory scale (10kW$_{SNG}$ output power) that can be easily upgraded to a multi-tube reactor set-up (multi kW$_{SNG}$ or MW$_{SNG}$ output power) by numbering-up the reactor tubes. Synthetic gas mixtures can be dosed into the laboratory plant while operating conditions as pressure level, gas hourly space velocities (GHSVs) and the reactor cooling temperature can be set. The axial temperature profile in the catalyst bulk is measured with eight thermocouples and the output product gas concentration is analysed with an infrared and heat conductivity gas analyser.

A schematic sketch of the cooled double jacket reactor with the oil thermostat can be seen in Figure 1.

For a realistic evaluation and validation of the conducted experiments, a 1D plug flow reactor (PFR) model has been set up to serve as comparison tool to effectively design tube-bundle reactors in industrial scale at a later stage. The details of the 1D PFR like model parameters and used intrinsic kinetic will be presented in detail at the conference.

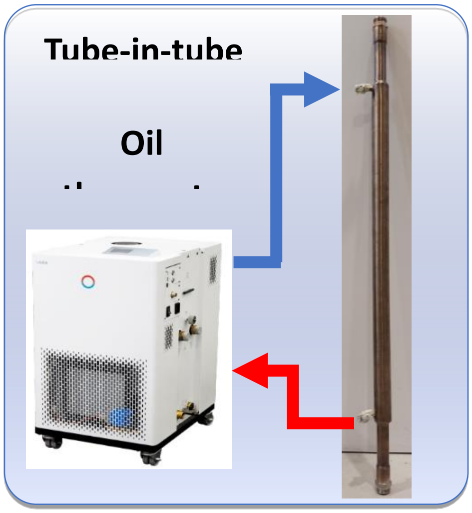

Figure 1. Laboratory set-up for catalytic methanation including a double jacket reactor and an oil cooling thermostat

3. Test runs in pilot plant scale

A typical biogas mixture (52vol.% CH_4, 48 vol.% CO_2) serves as input gas that is converted with a Hydrogen surplus of 4% to stoichiometry in the tube reactor. Very high gas hourly space velocities are investigated up to 20 000 h^{-1} at different pressure levels up to 10 bar while simultaneously the cooling temperature is varied in a reactor design with an inner diameter between 25 and 30 mm. Preferably, a single-stage methanation process is targeted to minimize the system complexity and the investment costs. Changes in the gas load (from low to higher gas hourly space velocities) should lead to consistent results in the produced synthetic natural gas (SNG) quality meeting gas quality criteria according to Austrian standards [1] (> 90 mol.% CH_4 and < 10 mol.% H_2) for grid injection.

4. Results

The experimental study of biogas methanation shows that optimal operation parameters including the pressure level, GHSV and cooling temperature need to be evaluated in a single-stage methanation process depending on the reactor design. The conducted biogas methanation experiments from the laboratory plant operated at a cooling temperature of 320°C are reproduced in the 1D plug flow model to verify the determined operating windows.

In the following graph, the dry product gas compositions of biogas methanation at different pressure levels and varying gas hourly space velocities are shown. The feed biogas mixture contains a share of 48 vol.% of CO_2 and 52 vol.% of CH_4, that is converted with a hydrogen surplus of 4% over stoichiometry.

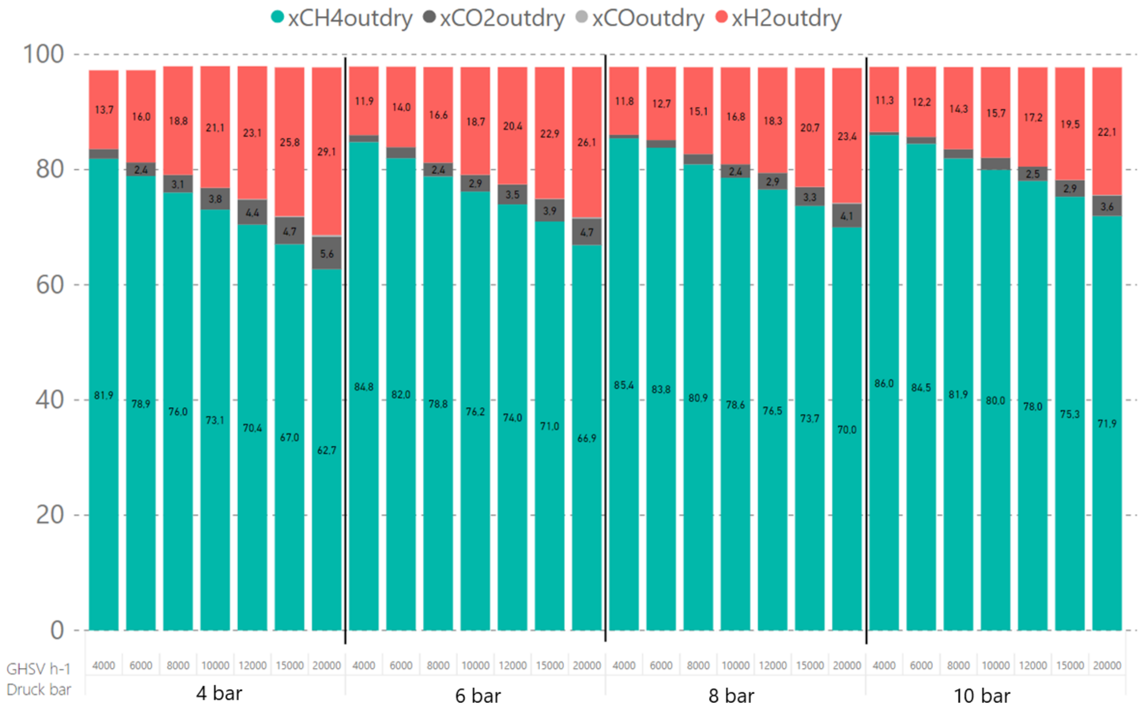

Figure 2. Dry product gas compositions of biogas methanation with 4% hydrogen surplus at different pressure levels and varied gas hourly space velocities

Especially for biogas methanation, a single-stage methanation process is targeted as less plant complexity immensely reduces capital expenditures in future megawatt projects. Figure 2 shows, that for the chosen reactor design single-stage methanation is challenging as the conversion rates drops with higher gas hourly space velocity resulting in a product gas composition that cannot be fed directly into the gas grid. The operating pressure affects the conversion rate in a positive way, meaning that higher pressures favour higher conversion rates. Only at low gas hourly space velocities (4 000 h^{-1}) and elevated pressures (8 and 10 bar), the SNG product gas composition nearly meets the Austrian gas grid feed-in quality criteria.

Compared modelled and experimental results of biogas methanation at different gas loads (4 000 and 12 000 h^{-1} - left and right, respectively) are depicted in the following axial temperature profile diagram. The oil cooling temperature is set to 320°C ensuring sufficient gas pre-heating upstream of the catalyst bulk for high reaction kick-off temperatures. It is also targeted, that the measured output temperature of the catalyst bulk equals the cooling temperature.

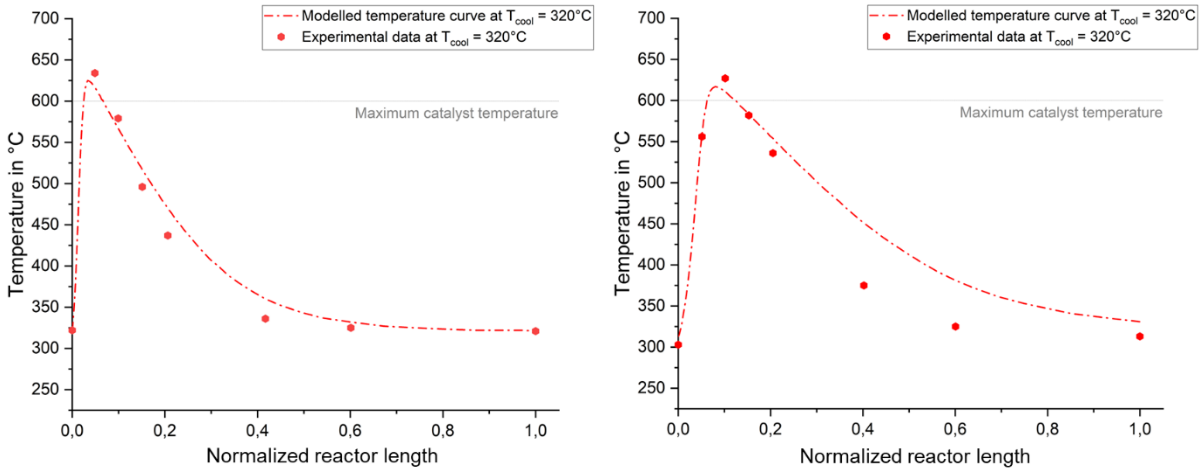

Figure 3. Compared temperature profiles of biogas methanation at two gas hourly space velocities (left: 4 000 h^{-1} and right: 12 000 h^{-1}) at 12 bar operating pressure from the 1D PFR model in matlab (line) and eight experimental temperature measurements (round markers).

At low gas hourly space velocities (4 000 h^{-1}) the alignment of the modelled and experimental temperatures corresponds well. At higher gas hourly space velocity (12 000 h^{-1}) the alignment match until the exothermic reaction peak. In the latter case, the cooling rate is underestimated from the model in comparison to the measured temperatures starting at a normalized reactor length of 0.4. In both cases, the modelled and experimentally measured temperature peaks surpass the maximum allowable catalyst temperature of 600 °C by nearly 20°C. A remedial action to reduce the temperature hot spots in the catalyst bulk is the reduction of the cooling temperature. A detailed analysis of the effect of the cooling temperature reduction on the single-stage methanation performance will be presented at the conference.

5. Summary and conclusions

Fixed bed reactors for catalytic methanation are characterized by challenging heat management. Especially in industrial scale applications stable operation without thermal runaway needs to be ensured. A cooled double jacket reactor set-up with an inner diameter between 25- 30 mm has been tested in a methanation pilot plant at MUL under varying operation parameters such as pressure level and catalyst load. As feed, a typical biogas mixture with a hydrogen surplus of 4% to stoichiometry has been used. The dry product gas composition and the measured temperature profile in the catalyst bed are used as evaluation parameters. In this paper, also the comparison between modelled and experimentally measured temperatures in the catalyst bulk is assessed.

The experimentally investigated variation of gas hourly space velocity and pressure level on the dry product gas composition illustrates that a single-stage methanation process in the chosen cooled tube reactor design is challenging. Only at very low gas hourly space velocities and elevated pressures (8 and 10 bar) the dry product gas composition nearly meets the gas grid feed-in quality criteria. For an optimization of the conversion rate - that automatically leads to product gas composition meeting the feed-in quality criteria also at higher GHSVs - the reactor diameter can be reduced slightly by about 5-10 mm still ensuring practical handling. This possible improvement of the reactor design will be tested in the laboratory pilot plant for future large-scale methanation projects.

The results from the 1D model accurately represent the axial temperature measurements in the catalyst bulk especially until the exothermic reaction peak is reached, both for low and higher gas hourly space velocities at a cooling temperature of 320°C. Only the cooling rate is underestimated from the model between a reactor length of 0.4 to 1, especially at higher gas hourly space velocities. As the maximum allowable catalyst temperature is surpassed at both gas hourly space velocities, the cooling temperature can be lowered (250-310°C) to reduce the local hot spot in the catalyst bulk.

References:

[1] Erdgas in Österreich - Gasbeschaffenheit ÖVGW G B210, ÖVGW Österreichische Vereinigung für das Gas- und Wasserfach, Jun. 2021.

11:10

Comparative Assessment of Solid Phase Adsorption Methodologies for Tar Quantification in Biomass Gasification

Presenting Author: Michael Kresta

M. Kresta [1,3,*], S. Hackl [1], A. Hofmann [1,2] and C. Pfeifer[3].
[1] Josef Ressel Centre for the production of powdered activated carbon from municipal residues, Department of Environmental, Process and Energy Engineering, MCI–The Entrepreneurial School, Universitaetsstraße 15, 6020 Innsbruck, Austria
[2] Department of Environmental, Process and Energy Engineering, MCI–The Entrepreneurial School, Universitaetsstraße 15, 6020 Innsbruck, Austria
[3]Institute of Chemical and Energy Engineering, University of Natural Resources and Life Sciences, Gregor-Mendel-Straße 33, 1180 Vienna, Austria
*presenter/corresponding author: michael.kresta@mci.edu

Introduction

The advancement of biomass gasification facilities necessitates characterizing their gas streams, typically comprising non-condensable compounds, steam, tars, particles, and other inorganic compounds. Tars, originating from the lignin component of biomass, typically consist of highly intricate and diverse mixtures of organic compounds, such as aromatics, phenols, bases, asphaltenes, preasphaltenes, and particulate matter with varying concentrations, influenced by the conditions of formation. The small amounts of tar by-products induce operating problems due to condensation in piping systems and linked gas turbines. [1] Consequently, minimizing tar content needs the ability to quantify tar levels in process streams. The time-consuming nature (long sampling time and laborious tar recovery) of tar measurement according to the Tar Protocol [2] CEN/TS 15439 is a major bottleneck in the analytics. The SPA method (solid phase adsorption), developed by Brage et al. at the Royal Technical University of Stockholm (KTH) [3, 4], is considered an alternative primarily due to shorter sampling time, lower cost of sampling equipment, lower amounts of solvents and ease of handling in comparison to wet chemical tar analysis. This method involves the adsorption of tar components onto a solid phase. The selection of the suitable sorbent is of high importance. The typically used LC-NH2 (SUPELCLEAN LC-NH2) cartridge accuracy was verified through laboratory tests, indicating adsorption of tar species except benzene and toluene, which exhibited notable breakthrough. [5, 6] The technique offers a reliable measurement range from xylene/phenol to pyrene, with promising results showing enhanced retention of naphthalene and benzene. Yet the SPA method's uncertainties and limitations in capturing heavy tars and benzene, toluene, xylenes (BTX) compounds highlight the need for further investigation and consideration of alternative methodologies.

Given that the typically employed NH2 matrix is polar, the strongly non-polar CHROMABOND C18, an octadecyl-modified silica phase, appears to be a promising alternative for sampling the non-polar tars. This study aims to evaluate two SPA cartridges in comparison to the Tar Protocol, serving as a benchmark method. Importantly, this evaluation is carried out in the context of a pilot gasification plant, without the use of model substances. Specifically, the investigation aims to assess whether employing C18 addresses the limitations inherent in the SPA method.

Experimental

The used SPA tar sampling system is adopted from the one developed by the KTH and described in literature [3–6] for better reproducibility. The proven method uses a ball valve for sampling, which is connected to an 8 mm plastic tube with a septum. The gas sample is taken through the septum using a cannula, flowing product gas through the adsorbent at a rate of 50 mL/min for two minutes using a pump. In the course of this work, it was established that due to the low extraction volumes in a real product gas flow, individual measurements deviate greatly from each other due to the process-related fluctuations in the tar load. For this reason the sampling volume of product gas is increased. The modified setup additionally features a self-locking T-piece, ensuring the ideal position of the cannula at the center of the pipe. A vacuum pressure gauge controls the correct and complete suction of the specified volume. Following sampling, cartridges are sealed and stored in a freezer to prevent tar evaporation. The syringes are eluted with a 50:50 mixture of isopropanol and hexane and measured in an HPLC.

Tar samples were taken at four different gasification plants, three of which are commercially working with the floating-fixed-bed technology developed by Syncraft (power plants: IBK, FF and AH). The development of the adopted SPA method was performed on a fluidized bed pilot plant (plant S) using municipal waste wood from a recycling center. Tar measurements were always carried out downstream of a hot gas filter bevor, ensuring a gas temperature between 200 – 300 C. The Tar Protocol measurements were performed according to CEN/TS 15439 using impinger bottles in a cold trap with hexane and isopropanol sampling 300 l of product gas.

Results and Discussion

The primary issue associated with the SPA method proposed by KTH is the precise timing of the measurements. Given the inherent fluctuations in the product gas, which are pronounced in relation to the type of gasification and the biomass utilized, as well as the temporal nature of the process the 100 mL gas sample employed in this study resulted in strong analysis deviations. For this reason, the sampling volume and thus also the sampling time were expanded and tested experimentally with one, two and three standard liters of product gas. The results demonstrated that the measured tar concentrations in the product gas remained constant with increasing sample volume. In tests conducted with the NH2 matrix, a breakthrough of tars onto a second syringe in series was observed at 2 and 3 l, which was not evident when using C18. This suggests that the non-polar C18 cartridge exhibit superior adsorption performance. In the NH2 cartridges the bed material gets saturated and desorption of the tars occurs, as the concentrations are below the level of the one and two liter tests. Additionally, with tar concentrations below 350 mg/Nm^3, the gasifiers examined in the course of this work have comparatively lower loadings. In order to be able to adsorb larger tar loads without breakthrough, the use of C18 cartridges with a gas sample volume of 1 l is recommended.

A comparative analysis of the cartridge matrix was conducted by employing C18 and NH2 syringes one after the other. A total of 1 l of product gas was sampled for analysis. Naphthalene and benzene, which are usually the most abundant aromatic species in product gases [7] have been chosen as fingerprint substances for PAH (naphthalene) and BTX (benzene) in this work. Figure 1 presents the mean naphthalene concentration in the product gas. It is measured on three replicates with SPA C18 and NH2 cartridge and the Tar Protocol (TP) as a benchmark. In four out of thirteen measurements presented in Figure 1, the Tar Protocol measurements were omitted. This decision was strategic, considering the intensive nature of the Tar Protocol procedure, and the focus at that phase was on developing the SPA method. The results demonstrate a good agreement between the naphthalene concentrations measured with the Tar Protocol and the SPA method, with both NH2 and C18. However, it can be seen, that the

C18 cartridges exhibit higher tar concentrations, compared the NH2. Of the 33 individual measurements, 85 % of the C18 measurements exhibited higher values than the NH2 cartridges, measured in direct succession. In Figure 1 it is also evident that the mean value of the C18 measurements is higher in most cases. Furthermore, a higher standard deviation can be observed when using the NH2 matrix. As shown in the experiments with increased gas volume, the difference is expected to be more pronounced with higher tar loads, as for e.g. in a traditional fluidized bed. As no heavier tars were found in the gasification plants sampled, neither with SPA nor the Tar Protocol, further tests are planned on a fluidized bed plant with a high tar content. It is expected that the C18 matrix is better suited to capture heavier tars due to its non-polar nature.

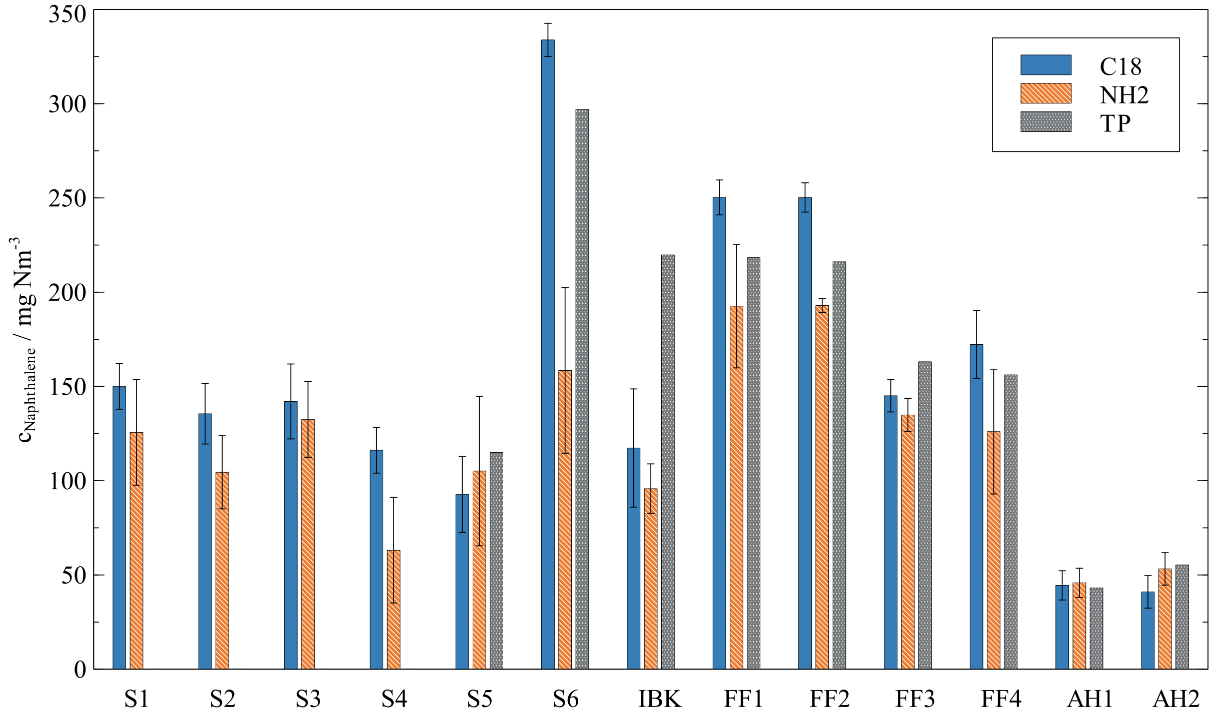

Figure 8:
Mean naphthalene concentrations in the product gas, measured with SPA C18 and NH2 and Tar Protocol

Benzene was examined as a representative substance for BTX, even though it is not considered as tar according to the most common classification systems by Energy Research Center of Netherlands (ECN) [8]. The Tar Protocol measurements consistently show higher benzene concentrations than the SPA method. This indicates that, as already confirmed in the literature [8, 9], the BTX compounds are not adsorbed or volatilize from the cartridges and a precise measurement using SPA is not possible. The use of the C18 cartridge also shows no significant improvement. Overall, the SPA method used in this study demonstrated good agreement with the Tar Protocol detecting tars heavier than BTX compounds using both NH2 and C18. One drawback is its limited sampling volume, especially when tar loads fluctuate. However, its simplicity, speed, and portability make it well-suited for general process monitoring.

Conclusion

In conclusion, this study aimed to assess the effectiveness of NH2 and C18 sorbents for tar quantification in biomass gasification. Through a comparative analysis of solid phase adsorption techniques with the Tar Protocol as a reference, the findings highlight the potential of C18 as a promising alternative to NH2 for capturing tars. The expansion of sampling volume addressed some issues related to fluctuating product gas compositions. Despite good agreement between the SPA method and the Tar Protocol for PAH tars, benzene concentrations consistently showed higher values with the Tar Protocol. While the SPA method offers simplicity and portability for process monitoring, its limitations with fluctuating tar loads and BTX compounds underscore the need for further refinement and application-specific considerations. The results suggest that employing C18 may address some of the limitations inherent in traditional SPA methods, offering improved accuracy and reliability in quick tar quantification. Further research is warranted to fully explore the capabilities and limitations of C18 sorbents in biomass gasification tar applications.

Acknowledgement

The financial support by the Austrian Federal Ministry of Labour and Economy, the National Foundation for Research, Technology and Development and the Christian Doppler Research Association is gratefully acknowledged.

References:

[1] M. Cortazar *et al.*, "A comprehensive review of primary strategies for tar removal in biomass gasification," *Energy Conversion and Management*, vol. 276, p. 116496, 2023, doi: 10.1016/j.enconman.2022.116496.

[2] J. Neeft *et al.*, "Guideline for Sampling and Analysis of Tars and Particles in Biomass Producer Gases," in *Progress in Thermochemical Biomass Conversion*, A. V. Bridgwater, Ed.: Wiley, 2001, pp. 162–175.

[3] C. Brage and K. Sjöström, "Separation of phenols and aromatic hydrocarbons from biomass tar using aminopropylsilane normal-phase liquid chromatography," *Journal of Chromatography A*, vol. 538, no. 2, pp. 303–310, 1991, doi: 10.1016/S0021-9673(01)88851-8.

[4] C. Brage, Q. Yu, G. Chen, and K. Sjöström, "Use of amino phase adsorbent for biomass tar sampling and separation," *Fuel*, vol. 76, no. 2, pp. 137–142, 1997, doi: 10.1016/S0016-2361(96)00199-8.

[5] X. Meng *et al.*, "Tar formation in a steam-O2 blown CFB gasifier and a steam blown PBFB gasifier (BabyHPR): Comparison between different on-line measurement techniques and the off-line SPA sampling and analysis method," *Fuel Processing Technology*, vol. 100, pp. 16–29, 2012, doi: 10.1016/j.fuproc.2012.03.002.

[6] I. Ortiz, R. M. Pérez, and J. M. Sánchez, "Evaluation of the uncertainty associated to tar sampling with solid phase adsorption cartridges," vol. 57, pp. 243–248, 2013, doi: 10.1016/j.biombioe.2013.07.009.

[7] B. Dou, W. Pan, J. Ren, B. Chen, J. Hwang, and T.-U. Yu, "Removal of tar component over cracking catalysts from high temperature fuel gas," *Energy Conversion and Management*, vol. 49, no. 8, pp. 2247–2253, 2008, doi: 10.1016/j.enconman.2008.01.027.

[8] L. P. L. M. Rabou, R. W. R. Zwart, B. J. Vreugdenhil, and L. Bos, "Tar in Biomass Producer Gas, the Energy research Centre of The Netherlands (ECN) Experience: An Enduring Challenge," *Energy Fuels*, vol. 23, no. 12, pp. 6189–6198, 2009, doi: 10.1021/ef9007032.

[9] M. Israelsson, M. Seemann, and H. Thunman, "Assessment of the Solid-Phase Adsorption Method for Sampling Biomass-Derived Tar in Industrial Environments," *Energy Fuels*, vol. 27, no. 12, pp. 7569–7578, 2013, doi: 10.1021/ef401893j.

Poster Presentations

1) Solvent extraction of aromatic aldehydes from biorefinery side-streams

Presenter: Alexander Kaufmann

Alexander Kaufmann[1,*], Lukas Maier[1], Lars Häcker[1], Jacob Michael Mayer[1] and Marlene Kienberger[1]
[1] CEET – Institute of Chemical Engineering and Environmental Technology, Inffeldgasse 25C, Graz University of Technology, 8010 Graz
*alexander.kaufmann@student.tugraz.at

Lignin a complex bio-based macromolecule, separated during pulp production, where it ends up in a bio refinery side stream e.g. kraft black liquor, which is finally combusted to gain process energy. Instead of solely using the calorific value of lignin, it can be oxidized to aromatic aldehydes e.g. vanillin, that are used in everyday products from flavors of food to additives in cosmetics or as precursors for redox active species in aqueous redox-flow batteries [1].
Solvent extraction of produced aromatic aldehydes from said oxidized side-streams is a key unit operation in the whole process with room for optimization towards more sustainability.

Here we demonstrate a solvent screening, finding alternative solvents to commonly used industrial solvents e.g. benzene or ethyl acetate, for the extraction of aromatic aldehydes vanillin, syringaldehyde, and *p*-hydroxybenzaldehyde from acidic aqueous solutions.
Therefore, a solvent screening by extractions with a model solution was done and finally selected solvents were applied on process streams from lignin oxidation routes.
The solvent extractions were conducted in separation funnels mounted on laboratory shakers and different solvents like esters, ethers, terpenes and terpenoids as well as novel synthesized eutectic solvents were investigated. The analysis was done via developed methods for HPLC-UV, Karl Fischer titrations and Total Organic Carbon (TOC) analysis to determine the extraction efficiency of each solvent towards the aromatic aldehydes as well as the solvents mutual solubility.

Model solution-extractions show that the terpenoid geraniol exhibits low solvent losses of ≤ 0.5 vol.% at 25°C, at extraction efficiencies of 97.73%, > 95%, and > 93% for *p*-hydroxybenzaldehyde, vanillin, and syringaldehyde, respectively [2]. Among all solvents that were applied to lignin oxidation streams, the terpene *p*-cymene was the only solvent to show selective extraction of vanillin and syringaldehyde from this highly complex matrix, achieving extraction efficiencies of roughly 90% for vanillin and 60% for syringaldehyde in one extraction step. The results of this work contribute to the field of solvent-extraction of aromatic aldehydes from acidic aqueous media.

References:

[1] W. Schlemmer *et al.,* "2-Methoxyhydroquinone from Vanillin for Aqueous Redox-Flow Batteries," *Angewandte Chemie (International ed. in English)*, vol. 59, no. 51, pp. 22943–22946, 2020, doi: 10.1002/anie.202008253.

[2] A. Kaufmann, L. Maier, and M. Kienberger, "Solvent screening for the extraction of aromatic aldehydes," *Separation and Purification Technology*, vol. 340, p. 126780, 2024, doi: 10.1016/j.seppur.2024.126780.

2) Advances in Photometric Fluoride Measurements in Effluent Fuel Cell Water

Presenter: Mathias Heidinger

Mathias Heidinger[1*], Daniel Sandu[2], Viktor Hacker[1], and Merit Bodner[1]
[1] Graz University of Technology, Institute of Chemical Engineering and Environmental Technologies, Inffeldgasse 25C, 8010 Graz, Austria
[2] AiDEXA GmbH, Bergmanngasse 45 T10, 8010 Graz, Austria
*presenter/corresponding author: mathias.heidinger@tugraz.at

The increasing focus on per- and polyfluoroalkyl substances (PFAS) by regulatory bodies, such as the EU's plan to ban PFAS products [1], has brought the topic into the public view. It is therefore important to have a reliable and suitable measurement method for the detection of fluoride in effluent fuel cell water.

This study is an improvement of the method from our previous work, in which we demonstrated an approach to detect fluoride in effluent fuel cell water, using a photometer [2].

Here we demonstrate, that by varying the reagent (SPADNS2) concentration, an increase in detection range or an improved sensitivity is possible. direct correlation between the reagent amount, detection sensitivity and linear range is measurable.

Through the variation of the reagent concentration, a direct correlation between the reagent amount, detection sensitivity and linear range is measurable. For a total sample volume of 1000 µL, varying the reagent amount between 50 and 200 µL changes the linear range to 0.5 mg L^{-1} and 5 mg L^{-1} respectively. This adjustment also has an impact on the sensitivity of the method, a reagent amount of 50 µL shows a 10-fold greater sensitivity (1.99 intensity / concentration) compared to 200 µL, where it is reduced to 0.20.

We have demonstrated the versatility of the photometric method in terms of adaptability for different concentration ranges. By adjusting the reagent amount to specific concentrations, and through the ability to readily change calibrations on the system, the method becomes suitable for a broader range of measurements.

This research is performed under the HyLife project (K-Project HyTechonomy, FFG grant number 882510) which is supported by the Austrian Research Promotion Agency (FFG).

References:

[1] European Chemicals Agency, ECHA, 22/03/2023
[2] M. Heidinger, E. Kuhnert, K. Mayer, D. Sandu, V. Hacker, and M. Bodner, “Photometric Method to Determine Membrane Degradation in Polymer Electrolyte Fuel Cells,” *Energies 2023, Vol. 16, Page 1957*, vol. 16, no. 4, p. 1957, Feb. 2023, doi: 10.3390/EN16041957.

3) Aging gracefully? Shelf-life investigations of catalyst ink for polymer electrolyte fuel cells

Presenter: Mario Kircher

Kircher, Mario[1, *]; Roschger, Michaela[1]; Koo, Wai Yee[2]; Blaschke, Fabio[1]; Grandi, Maximilian[1]; Bodner, Merit[1]; Hacker, Viktor[1].
[1] Institute of Chemical Engineering and Environmental Technology (CEET), Graz University of Technology, Inffeldgasse 25C, 8010 Graz, Austria
[2] Chemical Engineering Department, UTP Universiti Teknologi PETRONAS, Persiaran UTP, Seri Iskandar 32610, Malaysia
*presenter/corresponding author: mario.kircher@tugraz.at

Polymer electrolyte fuel cells (PEFCs) are recognized as sustainable energy converters. Today, wide-spread commercialization of PEFCs is hindered by cost-intensive manufacturing boundaries, most prominently high costs for catalyst material (Pt/C). Catalyst layers (CLs) are crucial for the performance and lifetime of a PEFC. They are formed by the deposition of catalyst ink (CI), a dispersion of the catalyst, a proton-conductive binder (e.g., Nafion) and a mixture of an organic solvent plus water. Unforeseen production stops of PEFCs or CI overproduction raise the question of storability of CI to avoid expensive disposal. [1]

Here, we demonstrate shelf-life investigations by phyisco- and electrochemical analysis for CI stored for up to four weeks [2]. The CI composition (Pt/C 20, Nafion N117, 2-propanol, water) was kept constant for all measurements. We identified UV-Vis spectroscopy as useful tool besides the determination of the Zeta potential to describe dispersion stability. Acetone was found as an oxidation product in the CI. The PEFCs performance is not harmed by CI storage after proper cell activation. At lower current densities, the power output is enhanced by a lowered charge transfer resistance over storage time which is attributed to an improved Nafion distribution within the CL. The pore structure of the CL becomes finer over time, especially after the addition of acetone to the CI. This leads, tendentiously, to a more hindered mass transfer of reactants at higher current densities. The best-performing PEFC (highest power output, lowest overall cell resistance) was fabricated from CI stored for four weeks. The results can be exploited in laboratory and large scale to prevent unnecessary waste and for considerations about CI preparation and storage. [1]

References:

[1] Berlinger, S.; Garg, S.; Weber, A. Multicomponent, multiphase interactions in fuel-cell Inks. *Current Opinion in Electrochemistry* **2021**, *29*, 100744. https://doi.org/10.1016/j.coelec.2021.100744

[2] Kircher, M.; Roschger, M.; Koo, W.Y.; Blaschke, F.; Grandi, M.; Bodner, M.; Hacker, V. Effects of Catalyst Ink Storage on Polymer Electrolyte Fuel Cells. *Energies* **2023**, *16*, 7011. https://doi.org/10.3390/en16197011

4) A versatile method for quantifying porous carbonaceous material in different wastewater matrices

Presenter: Christian Margreiter

Margreiter C.[1,2*], Hofmann A.[2], Wagner A.O.[2]
[1]Department of Microbiology, Universität Innsbruck, Technikerstraße 25d, A-6020, Innsbruck, Austria
[2]Josef Ressel Center for the Production of Activated Carbon from Municipal Residues, MCI Innsbruck, Maximilianstraße 2, A-6020, Innsbruck Austria
[*]christian.margreiter@student.uibk.ac.at

The continuous optimisation of water purification technology in waste water treatment plants (WWTPs) is of critical importance for the assurance of water quality and environmental protection. The incorporation of highly porous gasification residues (GR) and activated carbon (AC) as an additional purification step is providing a distinctive approach to tackle environmental issues e.g. associated with heavy metal and pharmaceutical residues in sewage. Due to the impact of GR and AC on process performance, residue monitoring and adsorption dynamics, it is important to verify the quantity and material transfer of these porous carbonaceous materials (PCMs), within sewage sludge and their behavior throughout different WWTP stages. Currently there are no established analytical methods for quantifying actual concentrations of PCM in difficult matrices like WWTP sludges. Therefore, the development of a simple and efficient method is needed. The present study investigated three different matrices with varying masses of GR and AC in known concentrations and applied several sample preparation approaches followed by total carbon analysis. The results demonstrated a linear correlation (R2 = 0.99) between PCM and TC content and was achieved through the combination of centrifugation, removal of excess supernatant, and slow drying. Thus, this method can be used to assess PCM concentrations ranging from 0.5 g l-1 to 20 g l-1 in activated sludge, denitrifying sludge, and anaerobic digestion sludge.

5) Production of activated carbon: Thermal activation of gasification char

Presenter: David Gurtner

David Gurtner [1,2*], Matthias Maurer [2], Michael Kresta [1,2], Angela Hofmann [2], Christoph Pfeifer [1]
[1] Institute for Chemical and Energy Engineering, University of Natural Resources and Life Science – BOKU, Gregor-Mendel-Straße 33, 1180, Vienna, Austria
[2] Josef Ressel Centre for production of activated carbon from municipal residues, Management Center Innsbruck – MCI, Department of Environmental, Process and Energy Engineering, Innsbruck, Austria
*presenter author: david.gurtner@mci.edu

The demand for activated carbon (AC) is increasing due to its great adsorption properties in water and gas treatment, which makes a renewable and sustainable production of AC crucial. A possible way is the physical activation of char from biomass. As precursor gasification carbon (GC), a by-product of wood gasification, could substitute fossil coal. The reaction mechanisms were investigated on lab-scale and findings transferred to a pilot-scale reactor, which is integrated in a commercial gasification plant. Due to the endothermal activation reactions with water vapour and CO_2, the addition of air is necessary for achieving high temperatures required for autothermal activation. Thus, in a preliminary step activation/re-gasification with only air is conducted. By adjusting the GC mass flow (15 $kg\,h^{-1}$) and the volume flow of air (13.4 $m^3\,h^{-1}$), temperatures of up to 1000 °C can be achieved. 21 w.% of the input GC is converted to gas with 22 vol.% CO. Due to high gas velocities, small particles are carried with the gas stream and only 35 w.% of GC exit the reactor. The additional introduction of CO_2 for activation reduced the temperature to an extent that proper activation could not be achieved. Thus, the injected gas mixture needs to be preheated to reduce the cooling impact of the cold gas entering the char-bed. For this approach, operational parameters still have to be found. For further development, the engine exhaust gas should be used as activation agent.

6) Characterization of pyrometallurgical systems by electrochemical methods

Presenter: Simon Moll

Moll, S.[1,*], Schlemmer, N. [1,2], Weiß, C. [1]
[1] Chair of Process Technology and Industrial Environmental Protection, Montanuniversität Leoben, Austria
[2] K1-MET GmbH Metallurgical Competence Center, Leoben, Austria
*presenter/corresponding author: simon.moll@unileoben.ac.at

Core metallurgical processes are often based on redox reactions – i.e. chemical reactions that involve electron transfer. To be mentioned exemplary, we may consider the reduction processes (regardless of the reducing agent, such as carbon, hydrogen, non-precious metals in zero-valent form, or electricity) as well as many refining processes. Frequently in pyrometallurgical operations metals are reduced from their oxidic precursors in molten state. Essentially, it can be said that whenever an element passes from the metal phase to the mineral or slag phase (or vice versa), a redox reaction system is present.

At the Chair of Process Technology and Industrial Environmental Protection we are concerned with the study of molten material systems at high temperatures, in particular with mineral melts and metallurgical slags. The aim is to mechanistically understand and offer options for a potential redesign of existing primary metallurgical processes. A key question is the discrimination of conduction phenomena (ionic and electronic conduction), which are causing measurable current flow through a liquid slag. Experimentally, we use the so-called van der Pauw - Ohta method. This method involves the measurement of the complex impedance of the melt over a wide frequency range (0.1 – 100 kHz) using a four-electrode bundle at different immersion depths. This enables the accessibility of the specific conductivity of the sample. A significant feature of this method is, that there is no need to determine a cell constant from the actual electrode geometry in submersed state, which would be extremely demanding in high-temperature applications. The difficulty in this context arises from the thermal expansion of the cell components in the inhomogeneous thermal field and the different electrode wetting by the sample melt compared to the aqueous calibration solution.

Currently, research questions also include measurements of the electromotive force of high-temperature galvanic cells and potentiostatic experiments. The aim is to determine activities and activity ratios, as well as species transport parameters in pyrometallurgical systems. The basic requirement for this type of experiment is an electrically continuous contact from the impedance spectrograph (used for conductivity measurements) or potentiostat to the melt. For potentiostatic measurements, a local separation of the oxidation and reduction half-reactions on suitable electrode surfaces is also required. In order to know exactly the polarization of the working electrode in potentiostatic experiments, a reference electrode is needed, providing a known reference potential. Within the context of high-temperature slag studies ($T \leq 1600$ °C) the development of reference electrodes permitting sufficient corrosion resistance during the measurements is of specific importance within our work area.

7) Experimental study on stirrer scale-up in the 2-20 liter range

Presenter: Thomas Senfter

Senfter, T.[1,*], Dörfler, L.[2], Berger, M.[3], Neuner, T.[1]., Kofler, T. [2], Mayerl C.[1] and Pillei, M[2].
[1] Dept. of Environmental, Process and Energy Engineering, MCI Innsbruck, Austria
[2] Dept. of Industrial Engineering & Management, MCI Innsbruck, Austria
[3] Dept. of Medical Technologies, MCI Innsbruck, Austria
*presenter/corresponding author: thomas.senfter@mci.edu

With the increasing individuality of products, the complexity of workflows in companies is constantly increasing. As a result, it is essential to develop the workflows used as efficiently and cost-effectively as possible. To identify all the necessary parameters of a process, laboratory tests are first carried out in practice. These should provide information about the range in which the optimal operating point lies. Once the process has been determined in the laboratory, it must be scaled up to an industrial scale to be profitable for the company. For a large number of chemical, physical and biological processes, mixing or stirring of the substances involved is necessary. This raises the question of which process parameters and properties of the substances influence the mixing result. The task of the research is to be able to give a statement on the application of these models in practice. This is to be achieved using an experimental investigation. This requires laboratory tests to be carried out to compare the results from theory and practice. The calculation models are adjusted in such a way that they exactly represent the stirrers available in the laboratory. 3 tank sizes (2.4 L, 5.7 L, 19.2 L), 3 different fluids (100% water, 37% water and 63% glycerol, 0.5 % water and 99.5% glycerol) as well as two different stirrer types (propeller, Visco Jet by VISCO JET Rührsysteme GmbH) are examined.

The results show that a geometric similarity of the stirring apparatuses to be investigated is essential for a valid calculation. Furthermore, the scaling task can only be applied if the properties of the fluids show a high similarity. The investigations have shown that the calculations have to be performed for each scaling case. A comparison with the literature or existing models is not useful because the parameters and substance properties have different effects on each stirring task. It is only possible to calculate the conditions accurately to a limited extent. For small tank size, 100% water and low stirrer speeds the calculated and experimental values differ by factors of up to >3. In selected ranges (19.2 L tank size, stirrer speed 300-800 1/min, 99.5% glycerol) the calculated and experimental values are in the same range. Both dimensional analysis and the Bueche-Theorem can provide a tendency for the necessary operating parameters, but no conclusion on the optimum operating point is possible with the investigations carried out in this work. At low speed of rotation speed, the torque measurement of the test setup is a critical factor. Further work on this topic should deal in more detail with the stirrer motors used and the data that can be supplied for the calculation. Furthermore, the implementation of a more precise measurement method for performance assessment would be beneficial in validating the findings of this study.

8) Life cycle-oriented cost assessment of an integrated energy system

Presenter: Doris Rixrath

Rixrath, D. [1,*], Sabo, E. [1], Schauer, R. [1] and Piringer, G. [1].
[1] FH Burgenland GmbH, Steinamangerstraße 21; A-7423 Pinkafeld
*presenter/corresponding author: doris.rixrath@fh-burgenland.at

This study describes a practical approach to the economic assessment method of Life Cycle Costing (LCC) and its application to an existing energy system. LCC is frequently seen as a key part of sustainability assessment, as it covers the economic aspect in the triple-bottom line concept of sustainability [1], [2], [3].

LCC is a well-known approach but there is very little information on how to apply this to assess energy systems. The objective is to first develop a practical version of the method and then to test its applicability on a case study. The case study energy system is a heating plant that supplies a district heat (DH) network in Neusiedl (Austria).

With this study we are able to demonstrate that it is possible to calculate life cycle costs of an integrated energy system which includes a biomass boiler, a back-up gas boiler, two water/water heat pumps, two air/water heat pumps which are supplied with electricity via a direct line from a nearby wind farm [4] .

The life-cycle oriented cost assessment follows the LCC method in combination with elements from the Environmental Life Cycle Costing (ELCC) [5], which largely follows the Life Cycle Assessment (LCA) methodology [6]. For the processing of the cost data, the net present value method is applied, as well as the ÖNORM guide-lines of ÖNORM 15459-1:2017 for life cycle costing and economic efficiency calculations.

Life cycle costs are calculated with €0.023 per MJ_{th} of heat for 2021. In the contribution analysis by component, air-to-water heat pumps (32.7% of total costs), biomass combustion (26.6%), and water-to-water heat pumps (23.4%) are the strongest cost drivers.

A sensitivity analysis where the investment costs are varied shows only a minor impact on the result. Significant impacts on the result are found for the variation of the electricity price or the discount rate.

The present LCC study is intended to contribute to the sustainability assessment of this innovative power-to-heat project. There is no direct comparability with literature possible, mostly they address single technologies [7] [8] [9]. The applicability of the method as well as benefits and limits of applying LCC method to a complex energy systems are a valuable outputs for further research.

References:

[1] J. B. Guinée *et al.*, “Life cycle assessment: Past, present, and future,” *Environ. Sci. Technol.*, vol. 45, no. 1, pp. 90–96, 2011, doi: 10.1021/es101316v.

[2] R. Heijungs, G. Huppes, and J. B. Guinée, “Life cycle assessment and sustainability analysis of products, materials and technologies. Toward a scientific framework for sustainability life cycle analysis,” *Polym. Degrad. Stab.*, vol. 95, no. 3, pp. 422–428, 2010, doi: 10.1016/j.polymdegradstab.2009.11.010.

[3] H. Mälkki and K. Alanne, “An overview of life cycle assessment (LCA) and research-based teaching in renewable and sustainable energy education,” *Renew. Sustain. Energy Rev.*, vol. 69, pp. 218–231, 2017, doi: 10.1016/j.rser.2016.11.176.

[4] 4ward Energy Research, “Projektvorstellung Hybrid DH Demo.“ *Youtube,* 2020, https://www.youtube.com/watch?v=f5P-sFpXud0.

[5] D. Hunkeler, K. Lichtenvort, and G. Rebitzer, “Environmental Life Cycle Costing.” *CRC Press*, 2008.

[6] International Standard Organization, “Environmental management — Life cycle assessment — Principles and framework (ISO 14040:2021).”, 2021.

[7] J.H. Miah, S.C.L. Koh, D. Stone, “A hybridised framework combining integrated methods for environmental Life Cycle Assessment and Life Cycle Costing”, *Journal of Cleaner Production*, vol. 168, 2017, pp. 846-866, doi: 10.1016/j.jclepro.2017.08.187.

[8] M. Ristimäki, A. Säynäjoki, J. Heinonen, S. Junnila, “Combining life cycle costing and life cycle assessment for an analysis of a new residential district energy system design”, *Energy*, vol. 63, 2013, pp. 168-179, doi: 10.1016/j.energy.2013.10.030.

[9] S. Paiho, S. Pulakka, A. Knuuti, “Life-cycle cost analyses of heat pump concepts for Finnish new nearly zero energy residential buildings”, *Energy and Buildings*, vol. 150, 2017, pp. 396-402, doi: 10.1016/j.enbuild.2017.06.034.

9) Mixed-Matrix Membranes on the way to Multi-Layer Membranes

Presenter: Jana Marx

Marx, J. [1,2,*],Rattinger, D. [1], Back, J. [1] and Spruck, M. [1].
[1] Department of Environmental, Process & Energy Engineering, MCI – The Entrepreneurial School, Maximilianstraße 2, Innsbruck, Austria.
[2] Institute of Textile Chemistry and Textile Physics, University of Innsbruck, Höchsterstraße 73, Dornbirn, Austria.
*presenter/corresponding author: jana.marx@mci.edu

The issue of micropollutants in the environment and the insufficient removal through the current wastewater treatment process is becoming an emerging threat to natural ecosystems [1]. Multi-channel mixed-matrix membranes, a filtration system that combines filtration and adsorption through embedding an adsorption material like powdered activated carbon particles into a polyethersulfone matrix, are a promising technology for the forth treatment step [2]. This technology already showed pathleading results in the removal of pharmaceuticals from wastewater and has a high potential for reusablity through chemical regeneration.

Based on these findings, it is aimed to encoporating alternative adsorption materials into the matrix of the polyethersulfone membranes. Therefore, graphene nanopellets, boronitride particles and two different powdered activated carbon particles activated with CO_2 and impregnated with zinc-chlorine are embedded into the polyethersulfone matrix. The particles were grinded to an average particle size similar to the embedded commercially available activated carbon particles (d_{50}=24 µm). The removal rate of six different compounds metropolol, carbamazepine, diclofenac, sulfamethoxazole, bisphenol A and benzotriazol is investigated using flatsheet mixed-matrix membranes with a thickness of 450 µm. The pure water flux is determined with tap water and the filtration is performed with a solution containing 15 mg/L of each substance over 60 min. The adsorption capacity of the substances was determined previously.

All different materials showed a higher specificity to some of the substances, which leads to the assumption, that the selectivity of the removal rate can be enhanced through embedding of different materials. The final goal is to combine these different adsorption materials to a serial process, through the production of multi-layer membranes. First experiments with pure polyethersulfone membranes showed the applicability of this production process. However, the method still has to be applied to different compositions of the polymeric solution. This technology is thought to play a significant role in the path towards a sustainable economy and reduce the eco-toxical effect caused by the emission of micropollutants.

References:

[1] Wilkinson JL, Boxall ABA, Kolpin DW et al. (2022) Pharmaceutical pollution of the world's rivers. Proc Natl Acad Sci U S A 119. https://doi.org/10.1073/pnas.2113947119
[2] Marx J, Back J, Hoiss L et al. (2023) Chemical Regeneration of Mixed-Matrix Membranes for Micropollutant Removal from Wastewater. Chemie Ingenieur Technik. https://doi.org/10.1002/cite.202300075

10) The reverse water gas shift reaction: Investigation of the reaction with nickel and perovskite based catalysts

Presenter: Marion Andritz

Marion Andritz[1,*], Christoph Markowtisch [1], Markus Lehner [1]
[1] Chair of Process Technology and Environmental Protection, Montanuniversitaet Leoben, Franz-Josef-Str. 18, A-8700 Leoben, Austria
*marion.andritz@unileoben.ac.at

The reverse water gas shift (rWGS) reaction represents a key technology for the catalytic conversion of CO_2 and H_2 to syngas, a feed gas for a Fischer Tropsch synthesis for e-fuel production [1].

The rWGS reaction is usually favored at high temperatures and low pressures whereas undesired side reactions, like methanation (CH_4) or carbon formation (C_{solid}) reduce the process performance time significantly. Operating the rWGS reactor at low temperatures lowers energy demand and reduces operating and investment costs due to simpler reactor design. Addressing these challenges requires a combination of innovative catalyst development and process engineering. Here, we demonstrate a comparison of commercially available nickel catalysts and novel perovskite catalysts for low-temperature catalysis identified by Lindenthal et al. [2] in the rWGS reaction on a laboratory scale.

The experimental setup consists of a gas mixing station (CO_2 and H_2), a quartz glass tube reactor, a cooler and a gas analysis. Operating conditions varied between 550 and 950°C and 1 to 8 bara. The influence of the operating conditions on the product gas composition and the selectivity of CO are compared for a Ni/Al_2O_3 and perovskite-based catalyst.

Results show the Ni/Al_2O_3 catalyst achieves thermodynamic equilibrium, favoring CO formation at high temperatures (950°C) and ambient pressure. In contrast, methanation reaction occurs notably at low temperatures up to 650 °C and 1 bara, leading to a significant increase in methane content with rising pressure and approaching thermodynamic equilibrium. However, the methanation reaction is suppressed on the perovskite catalyst. At 8 bara and 550 °C, perovskite catalysts exhibit comparatively low methane formation, maxing out at 2.7 vol.-%, in contrast to nickel catalysts with approximately 28 vol.-% at 8,000 h^{-1}. The results show that perovskite catalysts exhibit great potential for rWGS reactions related to power-to-liquid processes, leading to further investigations in an upcoming project.

References:

[1] Markowitsch C, Lehner M, Maly M. Evaluation of process structures and reactor technologies of an integrated power-to-liquid plant at a cement factory. Journal of CO2 Utilization 2023;70:102449.

[2] Lindenthal L, Popovic J, Rameshan R, Huber J, Schrenk F, Ruh T et al. Novel perovskite catalysts for CO2 utilization - Exsolution enhanced reverse water-gas shift activity. Applied Catalysis B: Environmental 2021;292:120183.

11) Utilizing Pressure-Driven Membrane Processes for Concentrating Sugar Solution

Presenter: Eva Walcher

Eva Walcher [1]*, Amal El Gohary Admed[1], Christian Jordan[1], Michael Harasek[1]
[1] Institute of Chemical Environmental & Bioscience Engineering E166, Technische Universität Wien, 1060 Vienna, Austria
* presenter/corresponding author: e1425978@student.tuwien.ac.at

In today's world, shifting from reliance on fossil fuels to embracing renewable energy sources is crucial. This transition requires careful planning and substituting traditional energy-intensive processes with sustainable and environmentally friendly alternatives.

Evaporation is a physical process that requires energy, often derived from fossil fuels, to facilitate the transformation of liquid water into vapor. This process is utilized in various applications to purify and separate water from impurities. Evaporation plays a crucial role in industries such as desalination, wastewater treatment, and the production of salt and other chemicals. Notably, membrane technology presents a viable alternative for water segregation and purification across different streams, characterized by lower energy consumption relative to evaporation. This research will explore the potential for replacing the concentration sugar solution by evaporation with membrane processes.

The research examined different pressure-driven membrane processes like reverse osmosis and nanofiltration to concentrate a model sugar solution while varying operational parameters. The study included testing various feed sugar concentrations to analyze how they affected the separation performance. The experiments were conducted on a lab-scale membrane unit, allowing for precise and controlled testing conditions.

12) Composition of textiles waste in Vienna

Presenter: Pablo Kählig

Pablo Kählig[1,*], Wolfgang Ipsmiller[1], Andreas Bartl[1], Jakob Lederer[1]
[1] CD-Laboratory for a recycling-based Circular Economy, TU Wien, Institute of Chemical, Environmental and Bioscience Engineering, Getreidemarkt 9/166, 1060 Vienna, Austria
*presenter/corresponding author: pablo.kaehlig@tuwien.ac.at

The European Commission's initiatives to implement a circular economy in the textile industry are evident, especially in the directive on the separate collection of textiles by 2025. In addition, circular fibre production depends on precise sorting and recycling processes to ensure the required purity of the input material stream. However, in order to enable an effective development of future processes, a knowledge base on the composition of these textiles is required. In this study we conducted sorting analyses of post-consumer textiles from mixed municipal solid waste and from collection containers of a charitable organization in Vienna with the aim to characterize these textiles according to defined attributes and to determine the potential for recycling in a closed product cycle.

For this purpose, textiles without label as well as shoes, bags & leatherwear, heavily contaminated and complex textiles were sorted out in a first step. In a second step, the remaining clothing and home textiles with label were characterized according to mass, type, colouring, composition according to the label, reusability and the presence of prints. The results show that the overall mass of textiles with label from both sources consists to a large extent of cotton fibres (over 60%). Furthermore, both sources consist of approx. 46% single-fibre material textiles without print, which would be easily accessible for recycling. For textiles that are composed of more than one fibre type, adequate material separation processes are required in addition to correct identification. These already exist for certain material blends like cotton / polyester, however for the most prominent material blend found in this study, namely cotton / elastane, such processes have yet to be developed.

Overall, it was found that there is a significant potential present for the recovery of secondary raw materials from waste textiles. However, further research into existing sorting and recycling processes is needed to fully exploit this potential.